Technical Report 451

Antenna System for LES-5

M. E. Devane
D. J. Frediani
B. F. LaPage
M. L. Rosenthal
A. Sotiropoulos

18 July 1968

Prepared under Electronic Systems Division Contract AF 19(628)-5167 by

Lincoln Laboratory
MASSACHUSETTS INSTITUTE OF TECHNOLOGY
Lexington, Massachusetts

The work reported in this document was performed at Lincoln Laboratory, a center for research operated by Massachusetts Institute of Technology, with the support of the U.S. Air Force under Contract AF 19(628)-5167.

MASSACHUSETTS INSTITUTE OF TECHNOLOGY

LINCOLN LABORATORY

ANTENNA SYSTEM FOR LES-5

M. E. DEVANE
D. J. FREDIANI
B. F. LAPAGE
M. L. ROSENTHAL
A. SOTIROPOULOS

Group 61

TECHNICAL REPORT 451

18 JULY 1968

LEXINGTON MASSACHUSETTS

ABSTRACT

The antenna system for Lincoln Laboratory's fifth experimental satellite (LES-5) is described. This is the first circularly polarized VHF antenna to be tested on an orbiting satellite. Coverage is omnidirectional in the equatorial plane. Design considerations are discussed, development of the component dipole and slot array elements is explained, and performance data are given for the final flight configuration.

Accepted for the Air Force
Franklin C. Hudson
Chief, Lincoln Laboratory Office

CONTENTS

ANTENNA SYSTEM FOR LES-5

I. INTRODUCTION

The fifth Lincoln Experimental Satellite (LES-5) is an all-solid-state VHF communications satellite which was placed in a circular orbit 1 July 1967 at a near-synchronous altitude of about 21,000 miles above the Earth. Drift of the satellite is about 30° longitude per day west to east. LES-5 is spin stabilized, at 10 rpm, with its spin axis perpendicular to its orbital plane which coincides with the Earth's equatorial plane. A magnetic torquing system stabilizes the satellite with its spin axis in the desired orientation. Spin was imparted as the satellite was ejected from the transtage of the Titan III-C launch vehicle after a flight from the Eastern Test Range.

The antenna system is noteworthy because it is the first circularly polarized VHF antenna successfully utilized on a communications satellite. It consists of two orthogonally polarized linear antenna arrays fed in phase quadrature to form the desired circular polarization. Although the LES-5 pattern coverage is omnidirectional, the antenna elements are similar to those planned for LES-6, which will have an electronically despun antenna. One of the experiments on LES-5 is a test of the switching circuitry which will cause the LES-6 steerable antenna beam always to point to Earth.

II. GENERAL DESCRIPTION

The size and shape of LES-5 is mainly determined by the desired orbital behavior and the available volume within the shroud of the Titan III-C launch vehicle. For a spin stabilized satellite with spin axis perpendicular to the plane of a circular orbit, the most natural shape is a right-circular cylinder. Because of the relatively low operating frequencies, the body should be as large as possible. The largest cylinder that could be accommodated by the shroud was about 4 feet in diameter by slightly less than 6 feet high.

LES-5 is basically a cylinder, 4 feet in diameter and 64 inches high, with eight equally spaced dipole antenna elements placed 6 inches from the cylindrical surface. The satellite is shown in Fig. 1. The outstanding external physical features are: the 4-inch wide "viewband" around the center, the 18-inch wide band of solar cells above and below the viewband, and the 12-inch wide "extensions" on each end.

The viewband is so called because it contains various optical sensors. Inside the satellite, just below the viewband, is an equipment platform which supports the communications, telemetry, beacon and radiometry equipment boxes, and interconnecting cables.

Each band of solar cells consists of eight identical curved panels with a $\frac{1}{4}$-inch gap between them. These gaps, plus similar ones in the extensions, are used as slot antenna elements. Together with the outer extension panels, the solar panels form the outside shell of the satellite

body. An inner shell is spaced $1\frac{1}{8}$ inches away from the inside surface of the outer shells forming an annular region. Each of these annular regions, above and below the viewband, is divided into eight backup cavities for the slot antenna elements. These backup cavities are so called because they serve to terminate the slot and prevent it from radiating inside the satellite. A slot which is thus constrained to radiate in one direction is called a cavity-backed slot.

The extensions provide the length needed by the cavities to permit propagation at the lowest frequency of operation: the "down" or transmit frequency. Thus, each slot element is a cavity-backed slot which, due to size limitations, operates just above the waveguide cutoff frequency. Sixteen of these slots are fed in phase and with equal amplitude signals to produce a linearly polarized omnidirectional field in a plane perpendicular to the spin axis of the satellite.

An orthogonally polarized omnidirectional field is produced by the eight equally spaced dipoles fed in phase. The desired circular polarization is obtained by feeding the two arrays through a quadrature (90°) hybrid. Note that the dipoles are stowed against the cylinder during launch, to meet the allowable volume requirement, and are deployed after separation of the satellite from the transtage.

Most of the satellite structural parts are fabricated from lightweight, high-strength aluminum sections. Main structural elements are fiberglass rings with U-shaped (channel) cross sections. Both the equipment platform and the solar panel construction feature a thin aluminum skin epoxy-bonded to an aluminum honeycomb core.

Total weight of the complete satellite at launch was about 230 pounds.

III. DESIGN CONSIDERATIONS

Antenna design was dictated mainly by the basic size and shape of the satellite, the desired omnidirectional circularly polarized radiation pattern, the frequency range, and the required gain. An important design feature was the utilization of the solar panels as portions of the antenna elements. Thermal and mechanical problems, in both the launch and orbital environments, were major considerations in the design of every part of the system. Originally, the satellite was to be less than 4 feet high to include only the viewband and the solar panels. Extensions were added when it became apparent that the size and number of antenna elements for the required gain could not be accommodated by the smaller cylinder. The antenna configuration was finally determined both by theoretical calculations and by experimental model studies.

After the decision was made not to use circularly polarized antenna elements (such as spirals and helices), various combinations of orthogonal linearly polarized elements were tried. One promising concept was to excite a square plate spaced a short distance from the cylinder in such a way that the two pairs of orthogonal slots, formed by the edges of the plate, would radiate circularly polarized energy. Thus, each solar panel would be an antenna element. However, model measurements indicated an impedance characteristic that would be very difficult to match over the required band. Also, the model showed that each element would have to be so large that only four could be arrayed around the circumference, and the resulting radiation pattern would not be sufficiently omnidirectional. It appeared that the proposed time schedule would not permit development of this new type of antenna, and the more conventional cavity-backed slot was adopted.

To accommodate the length needed by two rows of cavity-backed slots, the proposal was to have unfurlable or inflatable sections extend from both ends of the basic cylinder. This led to the idea of making these sections conical so that the satellite would be a large bicone antenna with

one row of feed elements around the cylindrical portion. However, the required gain could be obtained with two rows of slot elements and a set of eight equally spaced full-wave dipoles, as in the final design, and enough volume was finally made available on the launch vehicle to allow for fixed rigid satellite extensions and only the dipole elements then had to be made deployable.

Axial slots produced one of the two orthogonal polarizations and were essentially the only type antenna used to excite the circumferential polarization. A number of antennas were tried to produce the axially polarized component of the circularly polarized field. Some of these were: an array of monopoles on the top and bottom of the satellite, circumferential slots on the top and bottom and/or in the viewband (with and without erectable bicones), bent monopoles projecting from the top and bottom, the square-plate antenna which produced the two orthogonal polarizations, and a V emanating from the center of the viewband.

All these produced a fairly pure axial polarization. The general problem is that their maximum radiation was not in the equatorial plane, but the antennas produced much the same radiation as a $1\frac{1}{2}$-wavelength dipole, i.e., there are major lobes at $\Theta = 30°$ and $150°$ and a minor lobe at $\Theta = 90°$ or, at best, three equal peaks. Typical patterns are shown for a circumferential slot in the center (Fig. 2), circumferential slot top and bottom with bicones (Fig. 3), and an array of monopoles top and bottom (Fig. 4). The >1-wavelength dipole does have its peak in the equatorial plane and has a beamwidth of about 45° with a directivity of about 4 db. In addition, this dipole could be stowed, within the available volume, and then deployed in orbit.

IV. DEVELOPMENT

A. Cavity-Backed Slot Array

Expressions for the radiation characteristics of cylindrical arrays of axial and circumferential slot antennas were derived by Ricardi.[1]

For the axial-slot geometry shown in Fig. 5, the radiation fields are given by:

$$E_{\varphi}(\Theta, \varphi) = M_1 f_1(\Theta) \sum_{n=0}^{\infty} \sum_{p=0}^{N-1} \epsilon_n \frac{j^n b_p e^{j\psi_p} \cos n\,(\varphi - p\tau)}{H_n^{(2)'}(ka \sin\Theta)} \tag{1}$$

$$E_{\Theta}(\Theta, \varphi) = 0 \tag{2}$$

where

$$M_1 = \frac{e^{-jkr}\, L}{\pi^3 ar}$$

$$f_1(\Theta) = \frac{\cos(\frac{kL}{2})\cos\Theta}{1 - (\frac{kL}{\pi}\cos\Theta)^2}$$

$$\epsilon_n = 1 \ (n = 0) \quad , \quad \epsilon_n = 2 \ (n \neq 0)$$

$$k = \frac{2\pi}{\lambda} \quad , \quad \lambda = \text{wavelength}$$

n is an integer, N is the number of slots which are designated 0 to N − 1, b_p and ψ_p are the amplitude and phase of the voltage exciting the p^{th} slot, and $H_n^{(2)'}$ is the first derivative (with respect to the argument) of the Hankel function of the second kind.

Assumptions are that the excitation voltage is sinusoidally distributed along a slot which is much longer than it is wide, and the slots are arrayed in a perfectly conducting infinitely long circular cylinder. Good agreement between measured patterns of a finite cylindrical model and the computed patterns validate the assumptions.

For M rows of identical slots spaced S apart (between centers) and the relative excitation coefficient of the m^{th} row $a_m e^{j\beta_m}$, the far field is given by the previous equations when $f_{1a}(\Theta)$ is substituted for $f_1(\Theta)$ where

$$f_{1a}(\Theta) = f_1(\Theta) \sum_{m=0}^{M-1} a_m e^{j(\beta_m + mkS \cos \Theta)} \quad . \tag{3}$$

The foregoing expressions were used to compute radiation patterns and directivity of slot arrays fed in phase to produce omnidirective radiation with maximum field in the equatorial plane of the satellite. An array of eight equally spaced slots was found to produce a pattern omnidirective in the equatorial plane to within 0.3 db. Two such arrays, with slot pairs collinear, spaced almost 0.7λ between slot centers, produce sufficient directivity in the plane of the spin axis for adequate gain over the angle subtended by the earth.

Development of the slot array started with a model study of suitable cavity-backed slot elements. A considerable part of the effort was devoted to methods of matching the typically poor slot impedance characteristic to the transmitter and receiver over the desired frequency bands. Models of individual cavity-backed slots and arrays of such slots were used to measure the self and total impedance of mechanically suitable configurations. The final configuration was mainly determined by mechanical considerations and the resulting total impedance matched to the transmitter and receiver by a network. Total impedance includes the mutual impedance due to coupling between slots. Measured coupling between adjacent slots was about 15 db, so the coupling effect is significant.

Preliminary pattern measurements revealed a relatively high cross-polarized component for the slots, especially if they were fed off center. Therefore, a center feed was used and the cross-polarized field results in an effective loss of about 0.3 db. This loss is higher than that of the dipoles which had essentially no cross-polarized field.

Figure 6 shows the measured impedance characteristic at the center of the slot for the final mechanically acceptable slot and backup cavity configuration which was described in Sec. II. Because the slot impedance changes so rapidly with frequency, the decision was made to try to obtain a good match only at the transmit (TX) and receive (REC) frequencies and accept the resulting impedance at the telemetry (TLM) frequency and 250- to 280-MHz radio-frequency-interference (RFI) band.

Because of the high impedance at the TX and REC frequencies, an RF transformer with a large transformation ratio was needed. A so-called 4X transformer seemed suited to this application. A commonly used form of the 4X transformer is the three-conductor balun (balanced-to-unbalanced transformer) feed for a dipole.[2] The designation 4X comes from the fact that the transformation ratio is four times that of the usual quarter-wavelength (λ/4) transformer for a given change in characteristic impedance.

Figure 7 is a photograph of the 4X transformer feed, one of which is located in each backup cavity adjacent and parallel to each slot. It is located midway between the inside surface of the solar panel (which has been removed to show the transformer) and the mesh panel which is

the inner surface of the backup cavity. The 1-inch-square holes in these mesh panels permit more thermal radiation to take place from the inside surface of the solar panels than if solid metal were used. Thus, the solar panels can operate at lower temperatures in space, which results in higher conversion efficiency.

Each transformer is mounted on the metal channel section, as shown in Fig. 8, with its input (a TNC panel jack) projecting through the channel into the "inactive" region between backup cavities. In the figure, the mating TNC plug and its semi-rigid coaxial line can be seen. The transformer is a thin-wall aluminum tube 9/16-inch o. d. and 15 inches long, about 1/2 inch from the conducting surfaces of the backup cavity and the slot. About $\lambda/4$ from the connector, the tube is shorted to the channel. This is the feed point, and the tube between this point and the connector behaves similar to a $\lambda/4$ transformer with a characteristic impedance of about 120 ohms. In the region of the slot, this tube and the adjacent conducting surfaces of the channel and the solar panel form the equivalent of a three-conductor balun with a transformation ratio of about 20.

A short length of tubing extends beyond the feed point, as can be seen in Fig. 8. It ends just behind one of the fiberglass structural rings described in Sec. II. Therefore, it constitutes an open-circuited stub shunting the feed point and providing enough positive susceptance to make the admittance at the transmit frequency more nearly real before transforming.

Measurements showed that this feed transformer resulted in admittances at both TX and REC frequencies which could be matched to 100 ohms by a 25-ohm short-circuited stub about 0.10λ long, 0.14λ away from the load on 50-ohm line. To obtain the correct value of admittance at both frequencies, a short-circuited stub about $\lambda/4$ long at a frequency between the TX and REC frequencies was required at the connector end of the transformer. This was built into the otherwise unused inside of the feed tube. To compensate for dimensional differences between slots and backup cavities, this stub was made adjustable by providing an adjustable shunt capacitor at the connector end of the tube. This arrangement can be seen in Fig. 8, while Fig. 9 is a close-up photograph showing it in greater detail.

Thus, the complete matching network consists essentially of the transformer feed tube within the backup cavity at each slot, and two short-circuited stubs separated by a small length of line. There are two screw adjustments provided to tune each slot: one is the capacitor shunting the first stub, discussed in the previous paragraph; the second is a variable short on the 25-ohm stub. Also, the length of each slot can be adjusted, over a brief range of about 1 inch, by means of movable shorts across the gap between the extension panels near each end of the satellite. These three adjustments are employed to acquire about 100 ohms at each slot at both TX and REC frequencies. Then, to avoid using special high-impedance line, an upper slot and a collinear lower slot are fed in parallel through an approximately one-half wavelength of 50-ohm line. Thus, for each slot pair (consisting of an upper slot and a collinear lower slot), the resulting impedance at the paralleling tee connector is close to the desired 50 ohms at both key frequencies.

Beginning with the slot impedance characteristic of Fig. 6, the measured effect of the feed transformer is shown in Fig. 10(a). This includes the effect of the first stub and the adjustable shunt capacitor. Figure 10(b) shows the admittance at the second stub, and Fig. 10(c) shows the admittance of the collinear pair at the paralleling tee connector. Impedance data for the complete array are presented in Sec. V.

Total loss for the slot matching network was calculated to be less than 0.6 db. Table I lists the calculated losses in the major components of the network.

TABLE I
CALCULATED LOSSES OF SLOT MATCHING NETWORK

Transformer feed	0.09 db
First stub and adjustable capacitor	0.08
0.14λ line to second stub	0.08
Second stub	0.20
0.5λ line to paralleling Tee	0.09
Total	0.54 db

B. Dipole Array

As indicated in Sec. III, use of the >1-wavelength dipoles to produce the axial polarization was not an ideal solution; however, in considering the size of the satellite and the erecting of an antenna which would have its maximum radiation on the equator of the satellite, it appeared to be the only practical solution. Figure 11 shows the patterns of a dipole 1λ and 3λ/2 long; 3λ/2 is the upper physical limit of dipole length. At the same time, the impedance of a thin, center-fed dipole in free space (Fig. 12) is such that the least variation in impedance occurs near the 3λ/2 limit. A compromise based on measured patterns and impedance was made resulting in a dipole length, at the frequencies of interest, of 1.1 to 1.42λ.

A dipole is shown in Fig. 13. The feed line as it comes through the connector at the viewband is a thin strip of beryllium-copper (a) to provide the flexibility for storing. This is soldered to the thin-wall 0.060-o.d. aluminum tubing (b) which forms the dipole. The ends of the dipole are encased in fiberglass rod (c) which, in turn, is again mounted to a beryllium-copper strip (d) at each end of the satellite. For launch, the dipoles are bent to the satellite and captured top, bottom, and three places on the viewband.

The upper holding device (on each dipole) is a cam which pulls the dipole vertically, putting the bottom in tension against a beryllium spring and locking the three center holding devices in place. After the satellite is ejected, a squib is fired releasing the cam which permits the dipole to move down away from the upper and center locking devices, and allowing the springs to push the dipole into the erect position.

1. Impedance

The measured impedance at the input of a balancing, feed network, of one dipole, when all eight are excited in phase, is shown in Fig. 14. If a stub of appropriate length, impedance, and termination is added in parallel at the correct place on the main transmission line, it is possible to cancel the susceptance shown in the above plot at both the TX and REC frequencies. The stub will add capacitive susceptance at frequencies greater than resonance $[(f_t + f_r)/2]$ and inductive susceptance at lower frequencies. Two open-circuited stubs, each 1λ long in 15-ohm transmission line, were inserted at the appropriate place. Figures 15(a) and (b) are photographs showing a finished unit with the 50-ohm balancing line also attached; the calculated loss in this stub is 0.95 db. The calculated loss of an equivalent $2\frac{1}{2}\lambda$ open-circuited stub in 50-ohm line

is 1.08 db, so there was no advantage in using the longer stub; in fact, there was no room for the longer device cven if it had bctter performanee.

We planned to reduce the resultant impedanee to 50 ohms by using a transformer at each dipole. The flight antennas were slightly different electrically from the models (they appeared somewhat longer) so that thc use of the transformer was no longer appropriate. Figure 16 shows the impedance with the stubs in plaee. The nature of this impedance allows us to use just one 25-ohm cable at the input of the power dividers discussed in Sec. IV-C in place of the 35-ohm transformer mentioned. The impedance at the input to the power divider is shown in Fig. 17; the ealculated loss in the power divider is increased from 0.15 to 0.4 db by allowing a higher VSWR to exist throughout its length.

2. Patterns

The eight dipolcs were fed in phase to produce an omnidirectional pattern in the $\Theta = 90°$ plane, so the antenna directivity is a function of the Θ-plane radiation only. In this plane, we have seen that the radiation pattern is dependent on the length of the radiator. The length of the dipole was determined by taking a series of antenna patterns starting with the dipole length equal to $3\lambda/2$ at the shortest wavelength and reducing the overall length in small steps until fairly satisfactory patterns were obtained across the frequency band. Typical patterns for TX, REC, and the shortest wavelength arc shown in Figs. 18(a) through (c), respectively. Despite the fact that the three peaks are at the same level in Fig. 18(c), the directivity at this frequency is equal to or greater than that at TX.

Unfortunately, the flight-model antennas appeared to be slightly longer than the test models, probably due to the use of more and of a higher dielectric constant material as end supports than had been used on the model. The result was that the patterns at the upper end of the receiving band were poorer as shown in Fig. 19. Neither the TX nor the REC frequencies were noticeably affected.

C. Feed Network

As indicated in the LES-5 block diagram (Fig. 20), two 8:1 power dividers are nccded to feed the slot and dipole arrays with signals of equal amplitude and phase. Both coaxial and strip transmission-line networks were originally considered. Beeause of the limited mounting spaee available for the power dividers and the need for flexibility in some possible future modifications of the units, we decided to use coaxial 0.141-inch-diameter semi-rigid line. The design chosen uses only one length of nonstandard impedance line (35.4 ohms) and only a few lines of critical length. The divider is shown in Fig. 21 in sehematie form. The 50-ohm loads (slot or dipole impedances) in parallel become 25-ohm loads for the first junction. This 25 becomes 100 ohms when transformed through a $\lambda_o/4$ length of 50-ohm line. Thus, at the second junction, we have $Z_{in} = 100/2 = 50$ ohms. The load on the input junction is then $Z_{in} = 50/2 = 25$ ohms. This is matched to 50 ohms by a $\lambda_o/4$ transformer of characteristic impedance of $Z_o = \sqrt{25 \times 50} = 35.4$ ohms. This power divider gives a perfect match at only one frequency; however, for an $f/f_o = 1.10$, the theoretieal input VSWR varies from 1.11 to 1.33 depending on the line lengths at the first junction. The actual power dividers are shown in Fig. 22. This particular layout of the coaxial cables on the bottom of the platform is dictated by the presence of spacecraft structure and other components in the area. These dividers had the following measured properties over the 220- to 280-MHz band: 8:1 power split within ±0.15 db, maximum

VSWR of 1.34, maximum phase shift differential between outputs of ±2.0°, and an insertion loss (dissipative) of about 0.25 db.

D. Hybrid and Load

Referring again to the block diagram in Fig. 20, we see that the 90° phase shift needed to excite the antennas in quadrature for circular polarization is supplied by the 3-db hybrid (90°) junction. The hybrid also has the important function of providing some margin of safety should the dipoles fail to deploy. In this case, the reflected power from the dipoles would be divided in half on returning to the hybrid, so that in the worst-case situation only one-quarter of the incident power would be reflected back to the transmitter. The hybrid load shown would also absorb one-quarter of the incident power. During this type of failure, the slots would still receive half the total power and operate as in normal circumstances. If we had used a simple "Tee" junction to feed the slot and dipole antennas, we would need to supply the 90° phase shift by other means and, what is worst, the power split at the junction would depend on the antenna mismatch, thus giving us no assurance of a fail-safe operating condition. The amount of power dissipated in the hybrid load has been used as a diagnostic datum derived by sensing the temperature of the load.

The hybrid is a standard design quarter-wave coupled strip-line unit. Figure 23 shows the unit assembled and in parts. The two outside 3/16-inch thick and inside 1/32-inch thick, 2-ounce copper on Rexolite 1422 boards can be seen, along with the connector. The coupled strip was made a quarter-wave long in the dielectric at 250 MHz. The measured data are shown in Fig. 24. The power split is 3.0 ± 0.2 db from 200 to 300 MHz, and the dissipative insertion loss is about 0.05 db. The VSWR and isolation were considered adequate, even though they probably could have been improved with more work devoted to matching the connector and input of the hybrid.

The hybrid load is a commercial* 25-watt conduction-cooled unit which, though not originally designed for use in a space environment, was successfully qualified and flown. Figure 25 shows the load unit.

E. Triplexer

The triplexer[3] is a four-port passive microwave structure which provides a common antenna port for simultaneous operation at the transmit (TX), telemetry (TLM), and radio-frequency-interference/receive (RFI/REC) frequencies (see Fig. 26). The triplexer consists of three bandpass filters connected by appropriate lengths of transmission line. The TX and TLM filters have narrow bandwidths (approximately 1 MHz), while the RFI/REC filter operates over a 25-MHz bandwidth. All the bandpass filters use quarter-wave interdigital-type resonators, and were designed from the low-pass prototype.

A triplexer configuration is formed when three bandpass filters are combined through a common junction such that with simultaneous operation the overall response of each filter is relatively unaffected. In general, multiplexer designs are categorized into two types: contiguous, and noncontiguous. Contiguous refers to those multiplexers that have no guard bands separating the pass bands, while the noncontiguous multiplexer does have guard bands separating the passbands. The design of the contiguous class of multiplexers would be more complex than of the noncontiguous class because the interaction between filters would require additional

---

* EMCO T-4 50T.

compensation if one were to achieve a good impedance match at the input of a properly terminated multiplexer. Since the LES-5 multiplexer does have guard bands between the TX, TLM, and REC channels, the design procedure of combining the basic bandpass filters by using appropriate line lengths tied to a common junction is the most straightforward approach; then, each filter can be adjusted separately, simplifying the tuning procedure. Since the entire bandwidth of 25 MHz through the RFI/REC filter was expected to be somewhat degraded due to interaction effects, the approach used was to optimize the TX, TLM, and REC frequencies for the triplexer operation and accept the resultant RFI pass-band loss. The very high rejection (approximately 80 db) to the TX frequency presented by the RFI/REC filter is very nearly an open circuit at the reject frequency. By adjusting the junction line lengths, the approximate open-circuit impedances of each filter at the critical reject frequencies were transformed to the common junction.

Because of the resultant reduction in antenna system complexity, a common antenna terminal for the TX, RFI/REC, and TLM signals was considered highly desirable. However, this places the burden of signal separation on the triplexer system alone. The constraints on the triplexer are such that the TX frequency and any spurious outputs must be severely attenuated (~80 db) before reaching the receiver. For maximum efficiency, the REC, TLM, and TX filters must also have a minimum pass-band attenuation (≈0.5 db). In addition, the RFI filter bandwidth must have a sufficiently low loss across its pass band so that meaningful measurements can be performed. The basic filter specifications were derived from these and other similar considerations.

The junction is a copper-plated, gold-flashed aluminum box into which 0.141 semi-rigid coaxial cables are inserted and then soldered together. Special connectors are used which consist of the 0.141 cable outer conductor split four ways, then laid flat and soldered to the box. The cable is then firmly held in place with a flange. This technique was used to allow for easier adjustment of the cable lengths at the junction. Figure 27 shows the measured response curves of the triplexer. All the triplexer measured response curves show some variations from the smooth response curves of the single filters due to interaction effects between filters, through the triplexer junction.

V. PERFORMANCE

A. Radiation Patterns

Initial radiation patterns were measured with one-fifth scale models in the anechoic chamber at Lincoln Laboratory's Antenna Test Range facility. Figure 28 shows one of these models used during the development of the slot array. Patterns were measured at five times the operating frequencies with such models mounted on a low-dielectric-constant, foamed-plastic column. Thus, reflections presented little or no problems.

However, the full-scale development, pre-flight, and flight models had to be measured at the outdoor antenna test range, since the presently available VHF anechoic chamber was still in the planning stage at that time. To minimize reflections, the models were mounted as high as practical and the range was kept as short as possible, consistent with phase errors being below acceptable limits. By varying this range, the effect of reflections was noted and taken into account in the interpretation of the measured data and in the assessment of measurement error.

As shown in Fig. 29, the satellite was mounted about 21 feet above ground on the Scientific-Atlanta fiberglass model tower at the Antenna Test Range, and a plane reflector-backed dipole

was mounted at the same height on a wheeled metal staging. The wheels permit the distance between the two antennas to be changed readily. Both antennas have motorized drives controlled from within the adjacent building. With the satellite mounted so that the line-of-sight between it and the dipole passes through the center of the viewband perpendicular to the spin axis, equatorial plane patterns can be recorded by rotating the satellite about the spin axis. Polar-plane patterns can be recorded by rotating the spin axis in the azimuth plane. Conical cuts can be taken by fixing the azimuth angle at the desired value and rotating the satellite about its spin axis. For any of these cuts, the polarization characteristic (axial ratio) can be measured by rotating the dipole about the line-of-sight axis at a relatively high rate while the pattern is being recorded. Automatic, servo-controlled equipment is used to record relative power vs angle information. Such patterns were recorded at TX and TLM frequencies with the distance between antennas 13, 14, and 15 feet, and at REC at 13 feet.

Since the satellite antenna is a reciprocal device, patterns were measured by recording the RF energy received even at those frequencies for which the antenna is used for transmitting.

Response was measured with both linearly and circularly polarized radiation incident on the model. The latter was supplied by a helix antenna with an axial ratio of about 2 db; the former was from the rotatable dipole shown in Fig. 29. Both transmitting antennas were mounted in front of plane reflectors to provide an adequate front-to-back ratio and higher gain for the reduction of reflections from the ground and other surfaces. Rotation of the dipole about its polarization axis was remotely controlled. Therefore, any polarization cut could be readily recorded and, in general, response to two orthogonal polarizations (horizontal and vertical) was measured at each frequency of interest. By rotating the dipole at a constant speed continuously while the pattern was being recorded, we measured the response to any angle of linear polarization. Flight-model radiation patterns are shown in Figs. 30 through 46.

On the equatorial plane cuts, the horizontally and vertically polarized patterns are presented as well as the polarization pattern. More data would have been taken at the REC frequency, but when wind velocities began to exceed permissible values, the satellite was removed from the test mount.

Conical cuts were recorded (Figs. 44, 45, and 46) at 7° above the equatorial plane at the TX frequency. These represent the power received on earth 45° above the equator when the satellite is in orbit.

B. Polarization

Right-hand sense of circular polarization (IEEE definition) was confirmed for the satellite antenna system by the use of the right-hand helix transmitting antenna used for recording the circularly polarized patterns. An additional check was made by measuring the response when a crossed-dipole test antenna was used for receiving RF energy transmitted by the satellite. The axial ratio, and its variation with angle, is shown by the radiation patterns recorded while the linearly polarized transmitting dipole was spinning about its polarization axis (see Figs. 30 through 46). At the TX frequency, the axial ratio varies between 0 and 3 db as a function of the angle in the equatorial plane.

C. Gain and Effective Radiated Power

Gain was measured to both vertical and horizontal polarization, and the gain to matched polarization was calculated from these component gains. Most of the gain measurements were

made by noting the power received by the antenna model relative to that transmitted by the dipole. Two of these plane reflector-backed dipoles were constructed for use as gain standards, and their gain was measured by the identical antenna method. Thus, sufficient information was available to calculate gain with the range equation. A few measurements were made by the substitution method, and these corroborated those calculated. The gain is shown in Table II; the gain measurement error is estimated to be $\pm 1/2$ db.

TABLE II

GAIN AT THE INPUT TO THE HYBRID RELATIVE TO AN ISOTROPIC RADIATOR OF MATCHED POLARIZATION

Frequency (MHz)	Gain (db)
TX	+2-1/2
TLM	−1/2
REC	+2-1/4
260	−1/4
265	−5
270	−8
275	−11
280	−14

At each range and at the TX and TLM frequencies, the power received by the test dipole was measured. This was accomplished using a Hewlett-Packard HP 431C power meter that had been previously calibrated with an HP 8402A power standard. Received power was measured for both horizontal and vertical orientations of the test dipole for a reference position of the satellite; the effective radiated power (ERP) can be calculated for any angle from the measured radiation pattern, once it is calculated for the reference position.

For each measured received power P_R, the ERP is given by

$$ERP = P_T G_T = \left(\frac{4\pi r}{\lambda}\right)^2 \frac{P_R}{G_R} \tag{4}$$

where r is the range, λ is the wavelength, and G_R is the gain of the dipole. $P_T G_T$ is the product of satellite transponder or telemetry transmitter power and antenna gain which is, by definition, the ERP.

From known or measured quantities, the ERP for each linear (horizontal) and vertical polarization was calculated at the reference position of the satellite, and at 30° intervals in the equatorial plane. At each point, the ERP for matched polarization (generally elliptical) is the sum of the horizontal and vertical components. Thus, for the TX and TLM frequencies, twelve values of matched polarization ERP were obtained for each of the three ranges. At each 30° interval, the values for the three ranges were averaged to minimize reflection effects. Figure 47(a) shows the resulting plot for the TX frequency, and Fig. 47(b) for TLM. At the TX frequency, the resulting average ERP was 58.3 watts with a minimum of 55.5 and a maximum of

64.5 watts. The expected value was 56 watts. At the TLM frequency, the average was 0.470 watt with a minimum of 0.426 and a maximum of 0.514 watt. The expected value was 0.640 watt.

D. Impedance at Input

Impedance measurements were made with the model suspended from a gantry by a nylon sling so that all reflecting surfaces were more than one wavelength away. Measurements were made at the triplexer TX, TLM, and REC terminals at the appropriate frequencies. The impedance was also measured at the hybrid and at the power dividers. The VSWR at these locations is shown in Table III. Individual antenna element impedances had been measured previously after adjustment of the matching network.

TABLE III
MEASURED VSWR AT TRIPLEXER

Frequency (MHz)	VSWR	
	At Input to Hybrid	At Input to Triplexer
TX	1.15	1.14
TLM	1.20	1.17
REC	2.1	1.80
260	1.14	2.0
265	1.23	2.2
270	3.4	3.3
275	3.65	1.53
280	2.8	3.0

E. Post-Launch Data

After the successful launching of LES-5 on 1 July 1967, several communications experiments were conducted during the first visibility period, which lasted until 4 July 1967, for the Lincoln Laboratory ground terminal in Lexington, Massachusetts. These initial experiments confirmed that all systems were operating satisfactorily.

Since launch, successful communications have been carried out between various types of ground, sea, and air stations. Reliable information links have been established between relatively small, mobile terminals, in many cases for the first time.

VI. SALISBURY SCREEN TRANSPORTABLE TEST CHAMBER

A. Requirements for a Transportable Test Chamber (TTC)

Complete RF systems tests of communications satellites require that the antennas radiate in a free-space environment. Therefore, final RF systems tests are conducted at an antenna range or in an anechoic chamber. However, during qualification and environmental testing, such tests may be restricted due to the inaccessibility or unavailability of a test range or chamber. In addition, pre-flight systems tests must be conducted at the launch site, usually without

an RF anechoic chamber. These tests need yield only relative values of various parameters, the absolute values having been determined on the test range.

Where the radiation characteristics of the antenna system are independent of the spacecraft, e.g., aperture-type antennas operating in the upper microwave region, an RF absorbent "coupler" may be used. This coupler consists of a structure of convenient geometry lined with an appropriate absorbing material which is placed over the radiating element. A coupling or pickup probe incorporated in the structure permits closed-loop systems measurements. A multiplexer connected to the probe allows complete antenna systems tests. Such a coupling device was used successfully on the LES-1 and LES-2 antenna systems, as well as on the LES-4 transmitting antenna system.

B. Design Considerations

As a result of the operating frequency and the type of antennas employed on LES-5, the entire spacecraft is part of the antenna. This, plus the toroidal radiation pattern of the satellite, necessitated an anechoic chamber which completely encompassed the spacecraft. Since only relative measurements are required, no far-field criteria need be satisfied. The size of the chamber is then dictated by mechanical requirements. For accessibility, 18-inch clearance was allowed between the deployed dipoles and the inside of the chamber, making the minimum inside diameter 8 feet. A chamber lined with standard pyramidal absorber (carbon-impregnated foamed plastic) was considered, but published data indicated a minimum thickness absorber of 18 inches would be required to provide a reflected power level of -20 db. Such a chamber would meet the anechoic requirement, but the weight of the absorber and support structure would make it difficult to transport.

A solution to the transportability problem was the construction of an anechoic chamber employing the Salisbury Screen principle.[4] The Salisbury Screen is a narrow-band absorber formed by shunting a transmission line with an impedance which is equal to the wave impedance of the line with a short circuit one-quarter wavelength behind it. Theoretically, the Salisbury Screen absorber provides total absorption at the design frequency and a maximum reflection of -20 db over a 25-percent band, centered at this frequency, providing satisfactory absorption over the frequency range of interest. For free-space applications, 377 ohms per square material is commercially available. Due to the inherent difficulties in measuring absorbing material at UHF (antenna directivity, sample size in wavelengths, background reflections, etc.), no evaluation of the Salisbury Screen absorber was conducted. Since the material is easily fabricated, a cylindrical chamber was constructed with an outside diameter of 10 feet to obtain the desired 8-foot inner diameter. The 8-foot high outside cylinder is made of expanded aluminum. Figure 48 shows the complete TTC. The 377 ohms per square material consisted of 0.010-inch thick carbon-impregnated plastic film which was suspended on hooks at the desired spacing as can be seen in Fig. 49 which shows one of the four transportable sections into which the chamber is divided.

A probe was required to allow antenna systems tests. Since one function of the probe was to determine the phase relation between the dipole and slot components, a rotatable probe was incorporated. A dipole antenna with a coaxial rotary joint was used as shown in Fig. 50. To provide information of the entire toroidal radiation pattern, the satellite was mounted on an azimuth positioner as shown in Fig. 51. A DC-RF rotary joint in the azimuth turntable was used to supply DC power to the satellite transponder while under test. The test setup then consisted

of an azimuth turntable upon which the satellite was mounted with its spin axis perpendicular to the turntable, the Salisbury Screen absorbent chamber, and a rotatable probe mounted on the circumference of the screen centered on the satellite viewband. The azimuth rotator was mounted on a dolly to allow the satellite to be moved in and out of the chamber. For antenna patterns, the synchro information from the azimuth positioner was used to drive a rectangular pattern recorder which plotted amplitude information received from the probe antenna. As can be seen from Fig. 50, the probe was motorized and capable of rotating at 90 rpm to allow recording of polarization axial ratios, while the satellite was rotated at relatively slow speeds (≈1 rpm).

The entire chamber weighs 300 pounds and is composed of four sections which are easily transported without packaging or special handling, and the rotatable probe and curtains are easily removed and packaged for shipment. It is interesting to note that a 10-foot cubical chamber lined with 18-inch standard absorber material, later fabricated for impedance measurements, weighed 3200 pounds.

C. Radiation and Polarization Patterns

For vertical and horizontal orientations of the probe antenna, 360° equatorial patterns were recorded to measure the omnidirectivity of the satellite dipole and slot components. This provided a check of the power split between the slot and dipole arrays and the power distribution to the individual elements in each array. An additional 360° equatorial pattern with the probe antenna rotating allowed measurement of the polarization axial ratios to insure the phase quadrature relation between slot and dipole fields. These patterns were measured at TX and TLM using an external DC supply to power the transponder and the probe as the receiving antenna. Figure 52 shows a typical equatorial pattern of the flight satellite (measured in the Salisbury Screen test chamber) for the previously described orientations of the probe antenna. Since no malfunctions occurred in individual radiators of the flight antenna systems, these patterns were consistently reproduced throughout the test program.

D. Relative ERP and Transponder Tests

At a fixed equatorial position of the satellite, coupling measurements were made at TX, TLM, and REC frequencies from the output of the probe antenna to the antenna terminal of the satellite triplexer using precision coaxial attenuators. With external DC power applied to the transponder, RF power measurements were made at TX and TLM frequencies at the output of the probe antenna using the calibrated power meter. Applying the appropriate coupling values to these power levels yielded the TX and TLM power outputs under actual operating conditions. Since the power measured at the probe output is a function of the transponder output and the satellite antenna gain, it may be considered a relative ERP measurement. Such relative ERP measurements, made prior to and following the final free-space measurements of the flight satellite, were used as a reference. Since it was possible to have a malfunction of the antenna system which would not be observed in the radiation pattern, i.e., common to slots and dipoles, the relative ERP measurement was used as an additional check. If a decrease in power had been observed at the probe, a remeasurement of the coupling would ascertain which of the contributing factors had caused the decrease in ERP. As previously stated, no malfunction of the antenna system occurred and the power measurements were used to monitor the transponder output. Utilizing the probe antenna and the coupling to the triplexer at TX and REC, system sensitivity measurements were made. A known power level at REC was applied to the probe

antenna while the TX signal was received on it. Receiver sensitivity was measured for various bandwidths of the rceciver and modes of transponder operation by applying external commands.

E. Diagnostic Data

Diagnostic patterns were taken on the antenna model for various malfunctions of the antennas and feed network. Because of mutual-coupling effects, the perturbation of the antenna pattern was greatly dependent upon the type and location of the malfunetion, and a malfunction in a particular element did not always create the maximum perturbation at thc angular position corresponding to that element. Thcse patterns would have proven invaluable for immediately locating a malfunction on the flight model. Fortunately, the diagnostic patterns were never needed.

F. Summary

A log book containing antenna patterns, coupling, and later relative ERP measurements was kept from the conception of the pre-flight antenna model to thc flight model, following the flight model through its various environmental tests to final prc-launch tests at the Eastern Test Range. The Salisbury Screen test chamber provided the eapability for a full range of RF measurements on thc flight satellite from antenna pattern measurcments to complete transponder tests without the extensive handling and loss of time required in repeated utilization of the antenna range facility. During qualification, RF systems tests could immediately be conducted after each environmental test which would be indicative of the satellite performanee. Finally, the Salisbury Screen test ehamber provided the eapability for eomplete RF systems tests at thc Eastern Test Range prior to launeh.

VII. CONCLUSIONS

A fifth experimental satellite (LES-5) was designed, built, and tested by M.I.T. Lineoln Laboratory. The LES-5 antenna system was designed to operate in the VHF band, and extensive tests made both on Earth and in orbit proved the design to be suitable for space communications applications. Results of these tests are summarized in Table lV.

An average ERP of 58.3 watts at the TX frequency was obtained from pre-flight ground measurements made at thrce different distances between the satellite and thc test receiving antenna at the outdoor antenna test range. Differcnt distances are used to evaluate the effect of ground refleetions. At the TLM frequeney, the average measured ERP was 0.470 watt.

Radiation is eireularly polarized omnidireetional in the satellite's equatorial plane, with the axial ratio varying between 0 and 3 db at the TX frequency as a function of longitude. Maximum axial ratio is about 3 db at the TLM frequeney and about 4 db at the REC. Scnse of the polarization is right hand in aeeordanee with thc lEEE definition; this was measured using a right-hand helix as a test antenna.

In the polar plane, the measured radiation patterns show half-power beamwidths of 37° at TX, 35° at TLM, and 32° at REC frequencies. At the TX frcquency, the polar-plane powcr is down $\frac{1}{2}$ db 7° above and below thc equatorial plane.

The only unexpected result was the low ERP at the TLM frequency which is about 1.35 db below the anticipated value. Time and the weather did not permit repeating the measurements or investigating thc causè of the reduced telemctry performance. However, even the lowest measured telemetry ERP is still above the required minimum.

TABLE IV

SUMMARY OF LES-5 ANTENNA RADIATION CHARACTERISTICS

Terminal	TX	TLM	REC
ERP – to matched polarization with spin variation (watts)	64.5 (max) +0.45 db 58.3 (avg) 55.5 (min) −0.20 db	0.514 (max) +0.4 db 0.470 (avg) 0.426 (min) −0.5 db	–
Circularly polarized palar patterns	0.5 db dawn at ±7° 3-db beamwidth ≈ 37°	– 3-db beamwidth ≈ 35°	– 3-db beamwidth* ~ 32°
Axial ratio (warst case) (db)	~3	~3	~4

ERP ta Graund ar Airbarne Linearly Palarized Antenna

Linearly polarized antenna minimum ERP† (watts)	21.9 (max)	0.175 (max)
	19.8 (avg)	0.159 (avg)
	18.8 (min)	0.144 (min)

* Taken from pre-flight madel pattern data.

† −4.7 db dawn fram the circulary palarized ERP values.

Of interest is the linearly polarized ERP for use with ground or airborne systems employing linear antennas. With such an antenna oricnted to receive the minimum of the elliptically polarized field, the ERP would be about 18.8 watts at the TX frequency and 0.144 watt at the TLM frequency. With thc receiving antenna oricnted to receive the maximum field, thc ERP could be as high as 43 watts at the TX and 0.343 watt at the TLM frequencies.

Since launch, LES-5 has performed about as predicted in orbit. Several records were established for long-distance communications bctween relativcly small mobile ground, air, and sea stations.

REFERENCES

1. L. J. Ricardi, "Directivity of an Array of Slots on the Surface of a Cylinder," Technical Note 1966-52, Lincoln Laboratory, M. I. T. (10 October 1966), DDC 641959, H-748; also in Electron. Eng. 39, 578 (1967), DDC 668239.
2. H. J. Riblet, "Slotted Dipole Impedance Theory," Report 772, Radiation Laboratory, M. I. T. (21 November 1945).
3. A. Sotiropoulos, "LES-5 Triplexer," Technical Report 438, Lincoln Laboratory, M. I. T. (31 August 1967), DDC 823174.
4. W. W. Salisbury, "Absorbent Body for Electromagnetic Waves," U. S. Patent No. 2,599,944 (10 June 1952).

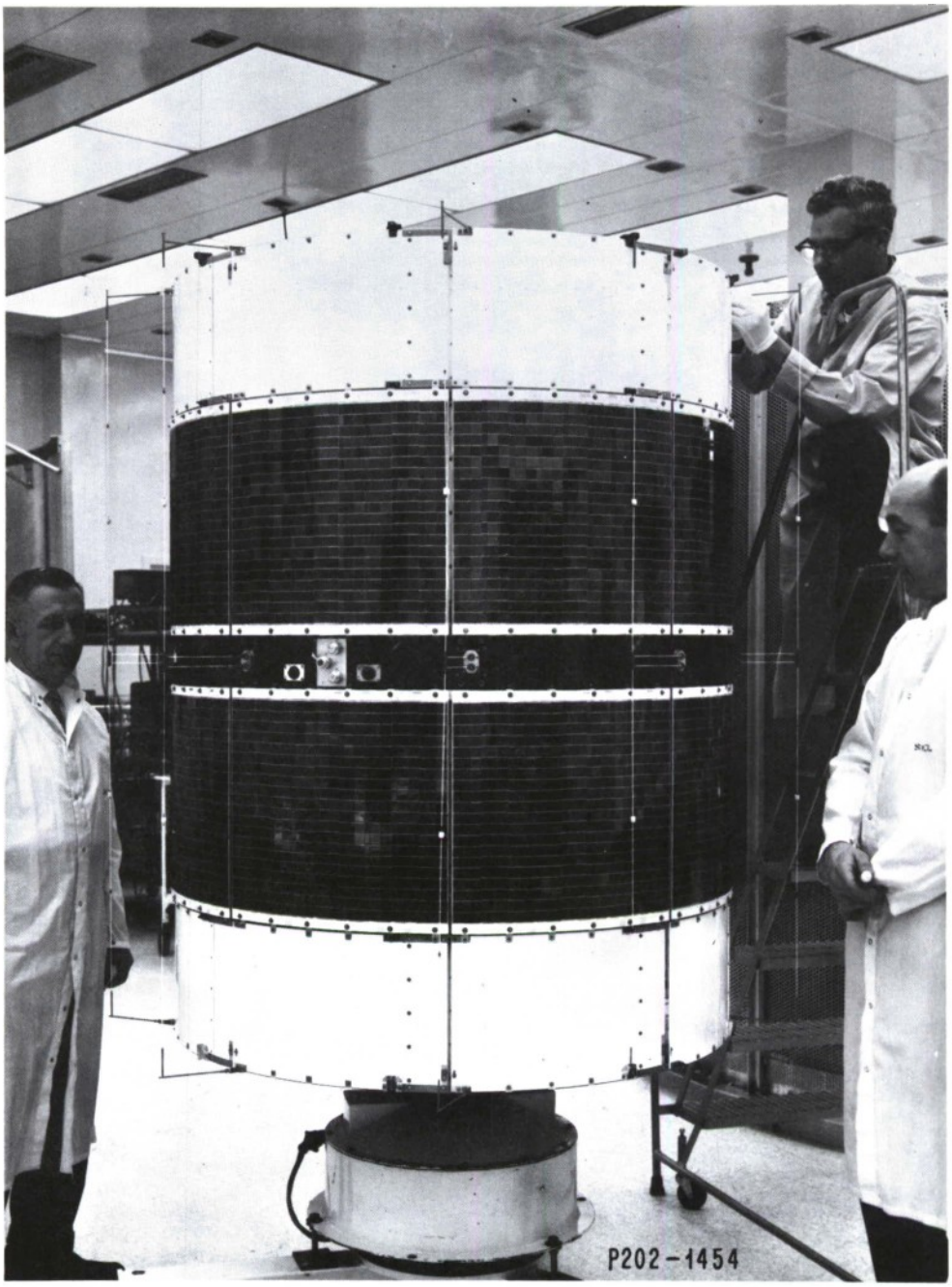

Fig. 1. LES-5.

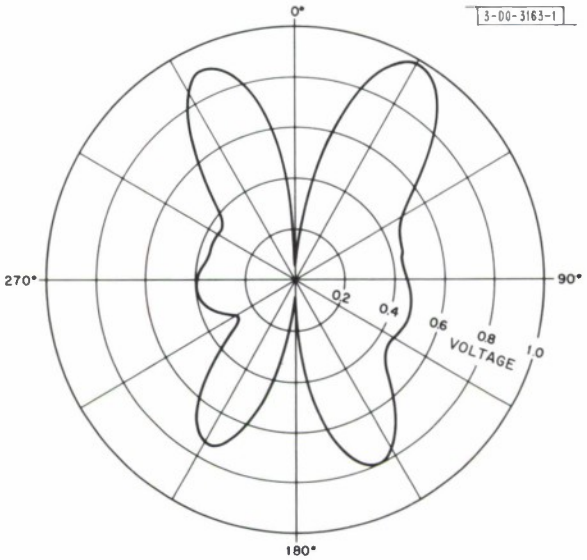

Fig. 2. Rodiotion pattern, circumferentiol slot in center of cylinder.

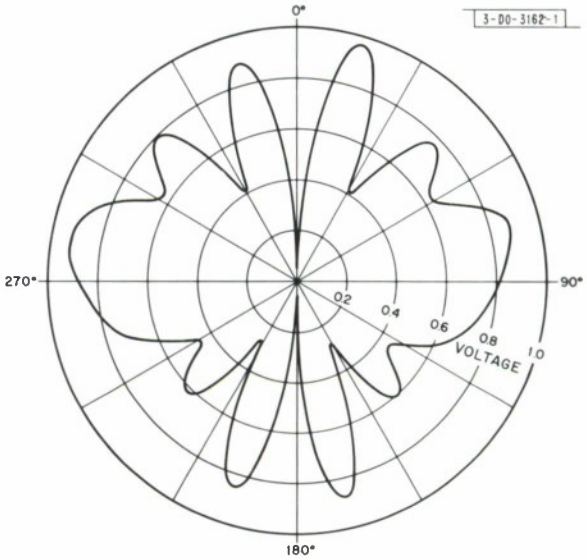

Fig. 3. Rodiotion pattern, circumferential slots top and bottom of cylinder with bicones.

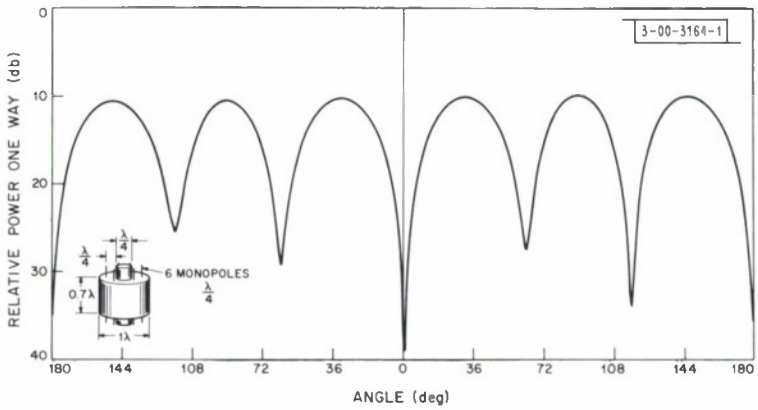

Fig. 4. Rodiotion pattern of arroy of monopoles on top ond bottom of cylinder.

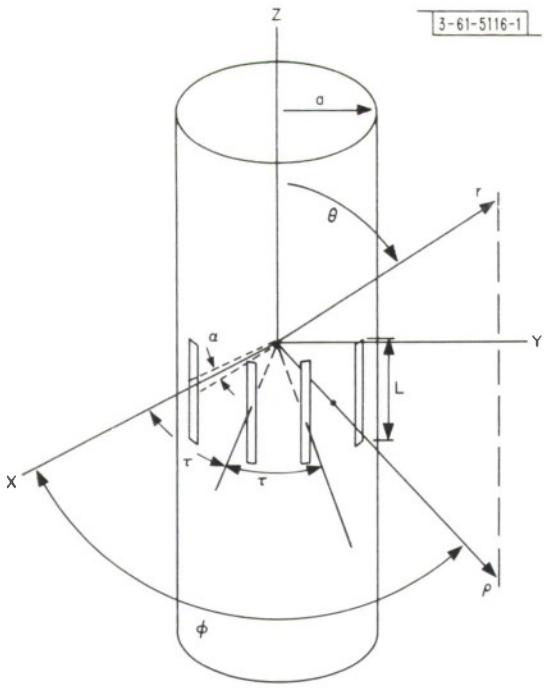

Fig. 5. Axial-slot geometry.

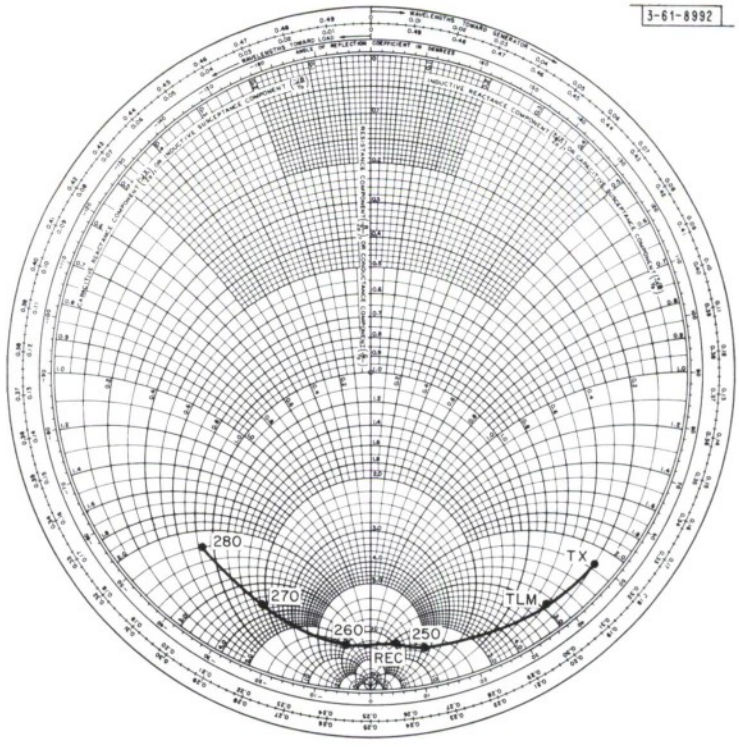

Fig. 6. Measured totol impedonce of typical slot.

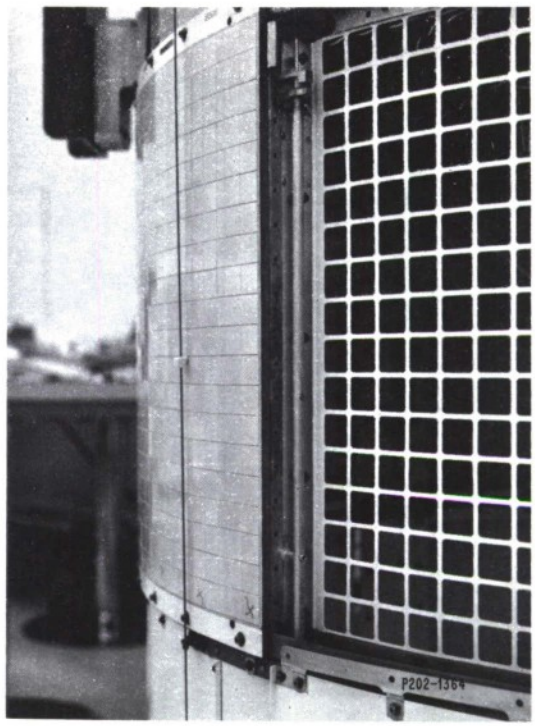

Fig. 7. Slot-feed transformer.

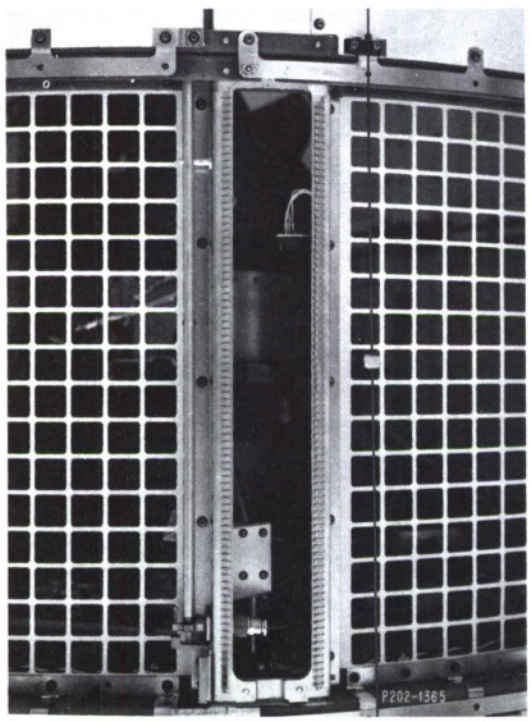

Fig. 8. Feed transformer, side view.

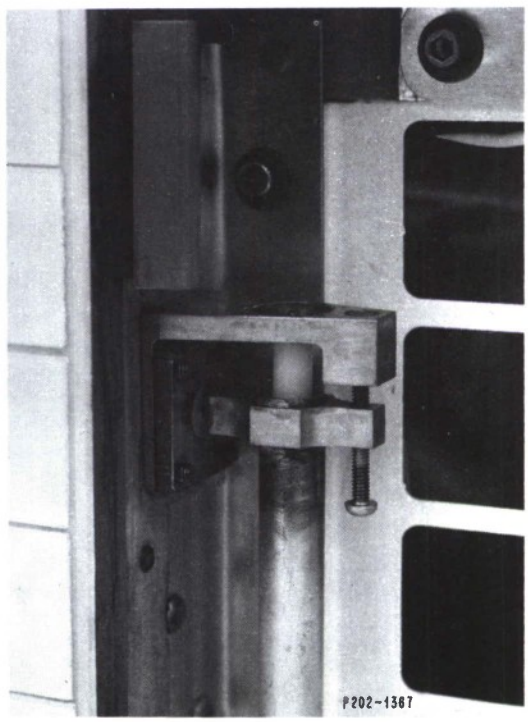

Fig. 9. Adjustable shunt capacitor.

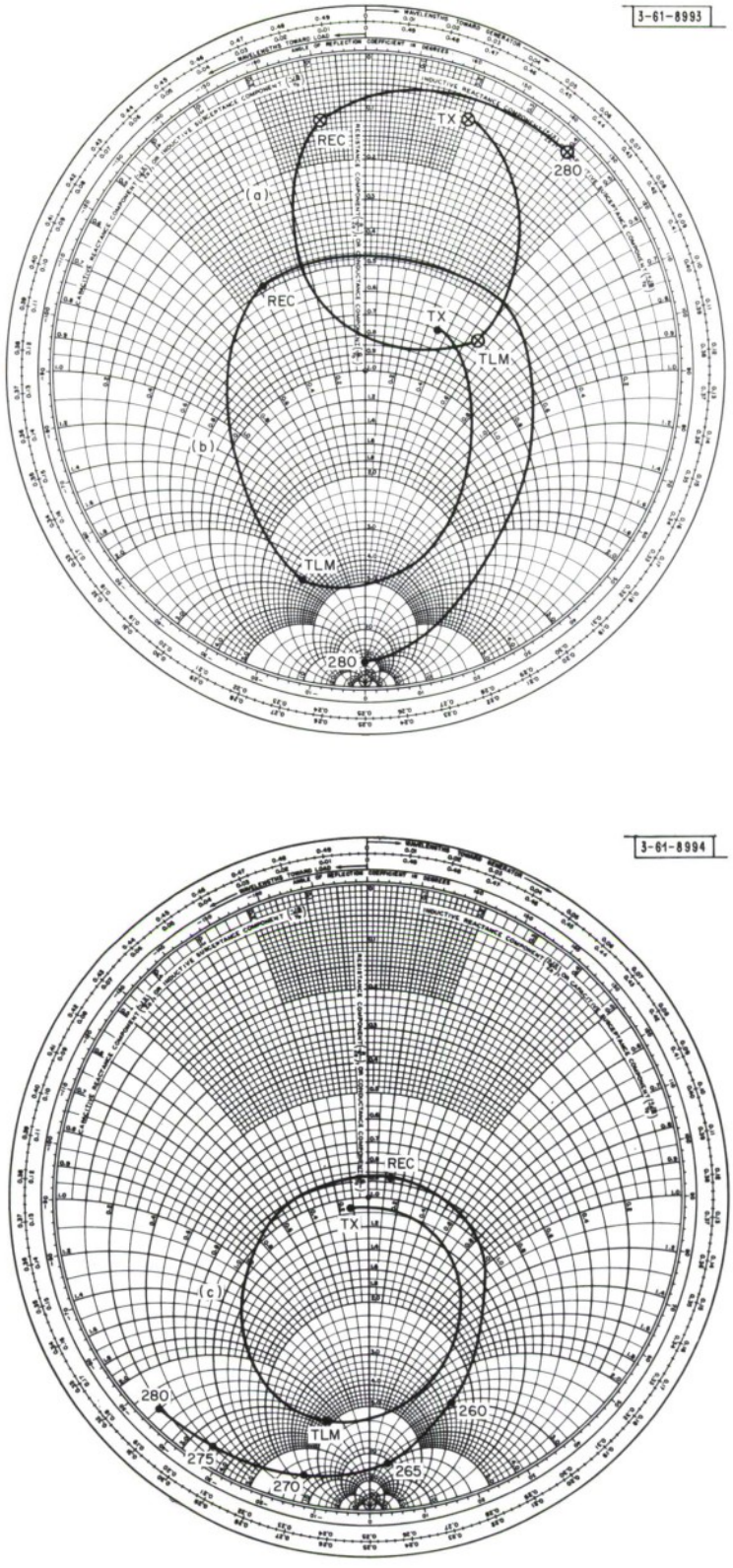

Fig. 10. Measured admittance (a) at transformer, (b) at secand stub, and (c) af callinear pair af slats.

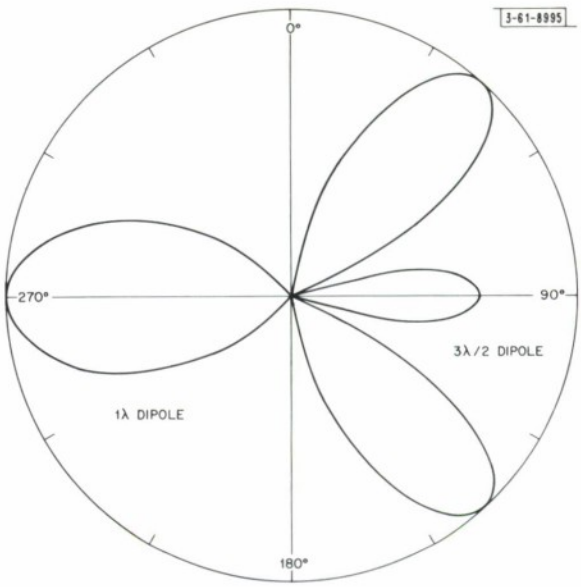

Fig. 11. For-field rodiotion potterns of 1λ ond 3λ/2 dipole. Cross section of figure of revolution shown.

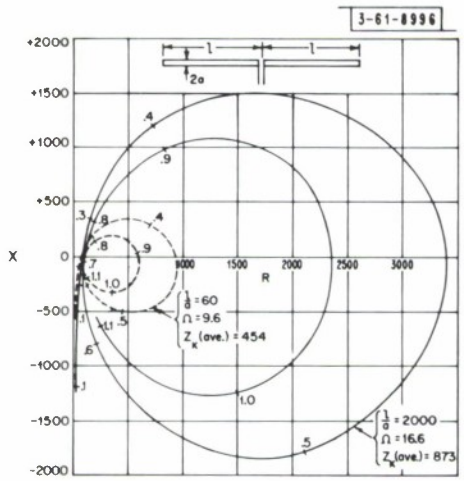

Fig. 12. Calculoted impedonce for cylindrical center-fed ontenno. [Reproduced with permission from J. D. Krous, Antennos (McGraw-Hill, New York, 1950), p. 242.]

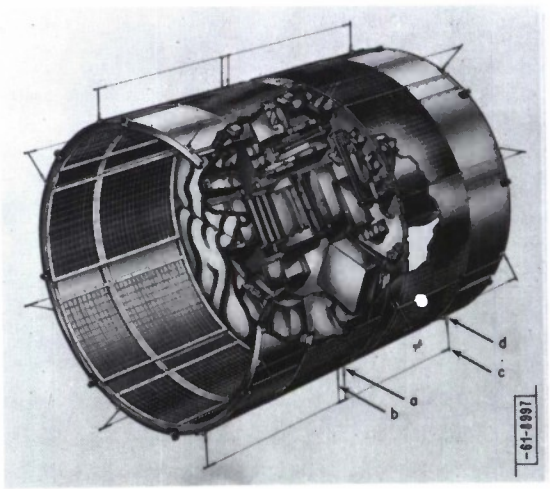

Fig. 13. Dipole with collouts.

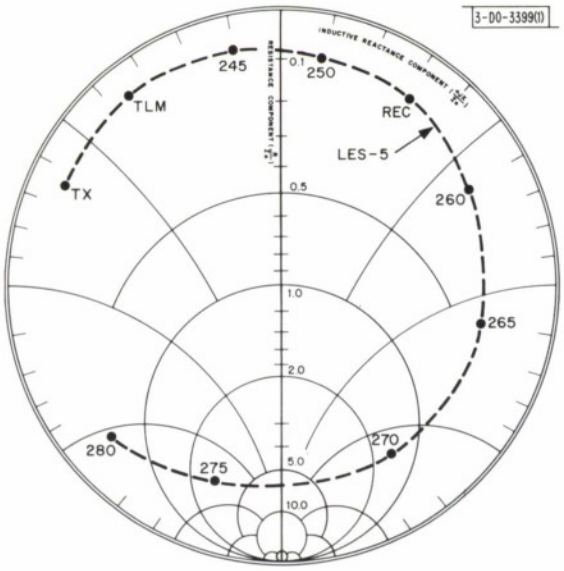

Fig. 14. Measured input impedance of 1-1/4 λ (at TX) dipale.

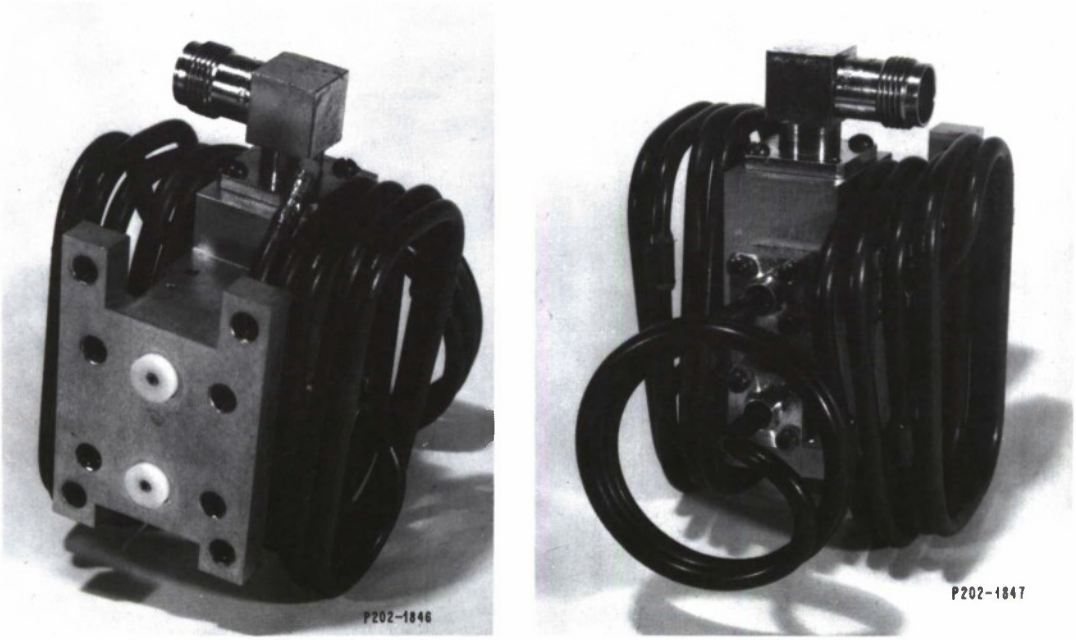

(a) (b)

Fig. 15. Matching device for dipales: (a) front view, (b) rear view.

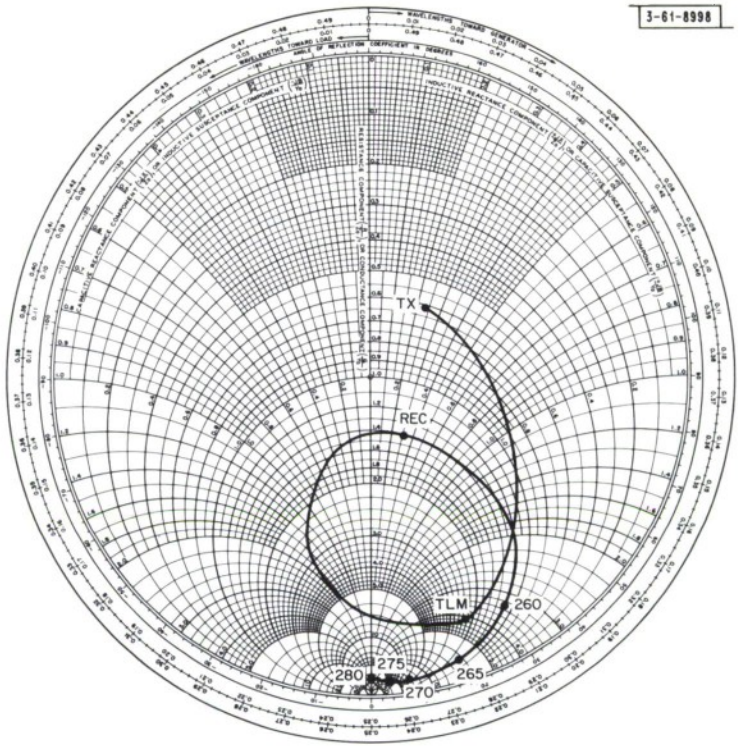

Fig. 16. Impedance of flight dipale at feed.

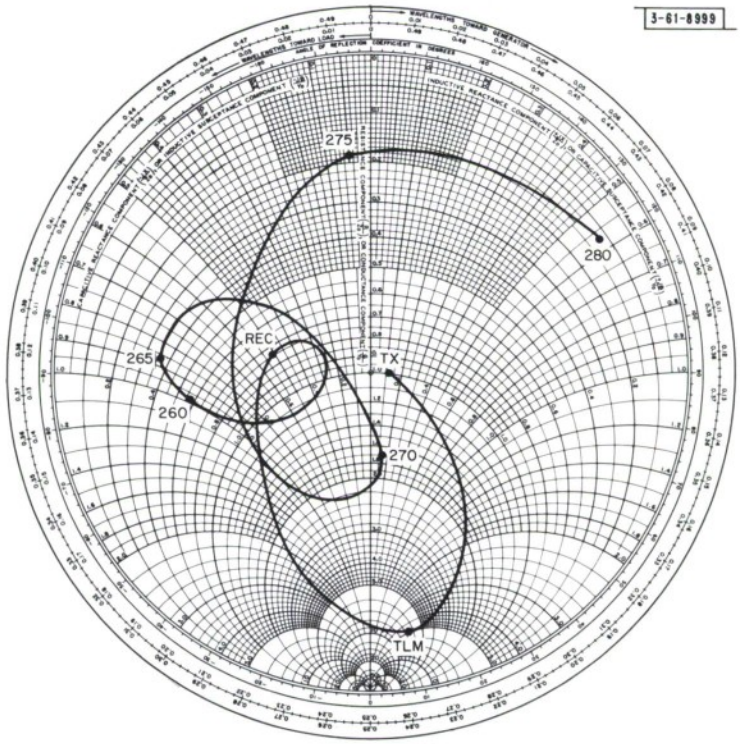

Fig. 17. Impedance at input to power divider.

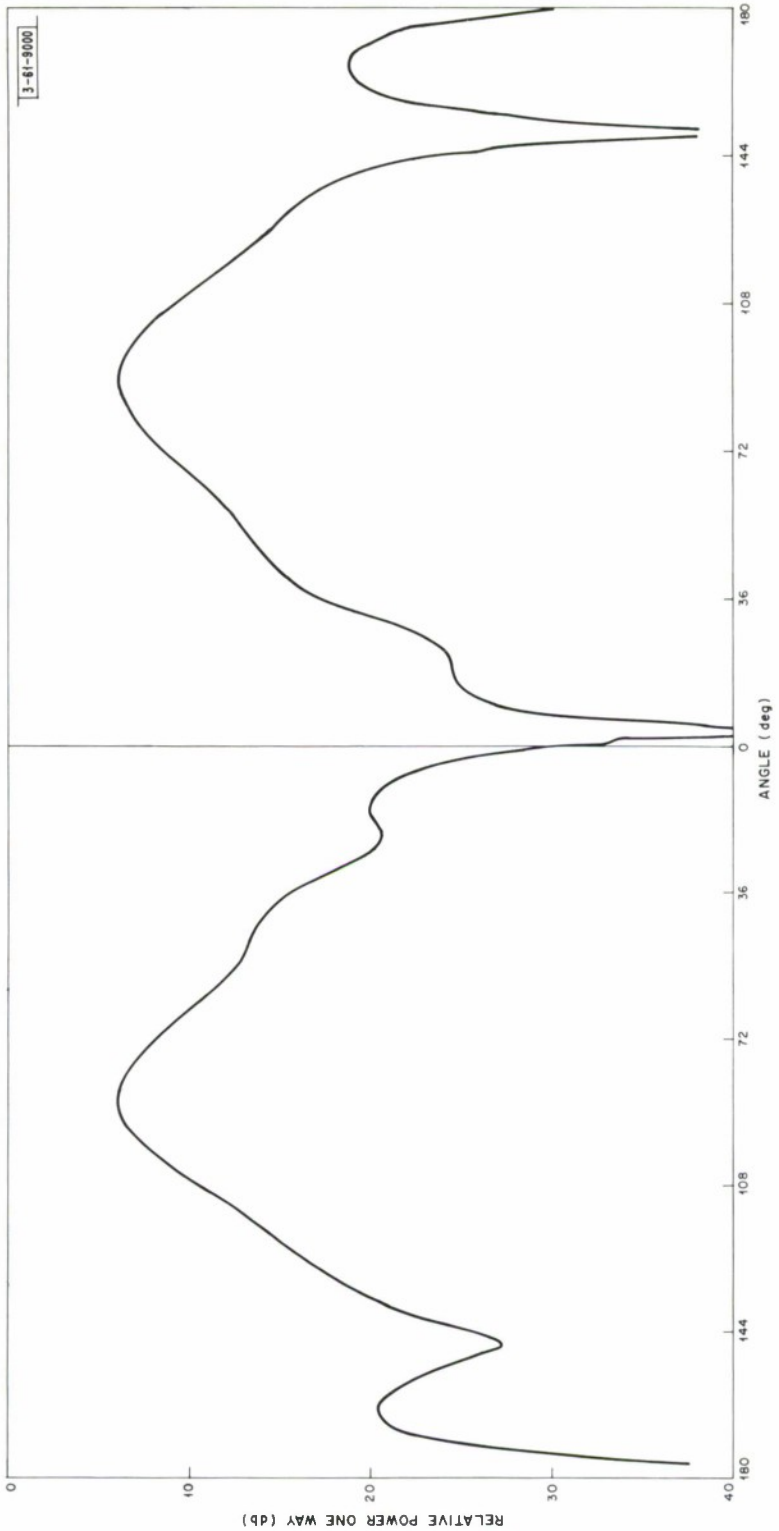

Fig. 18(a). TX pattern.

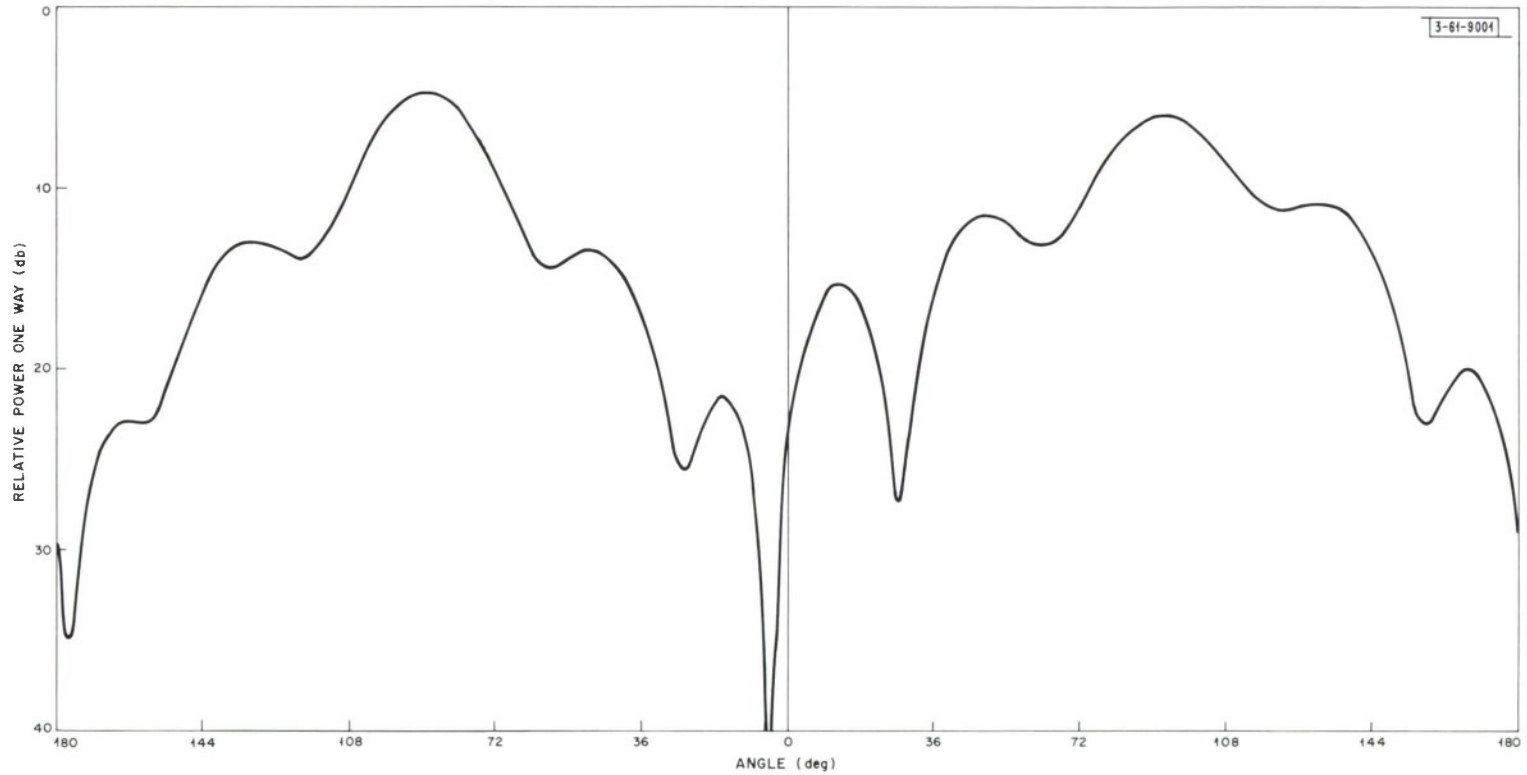

Fig. 18(b). REC pattern.

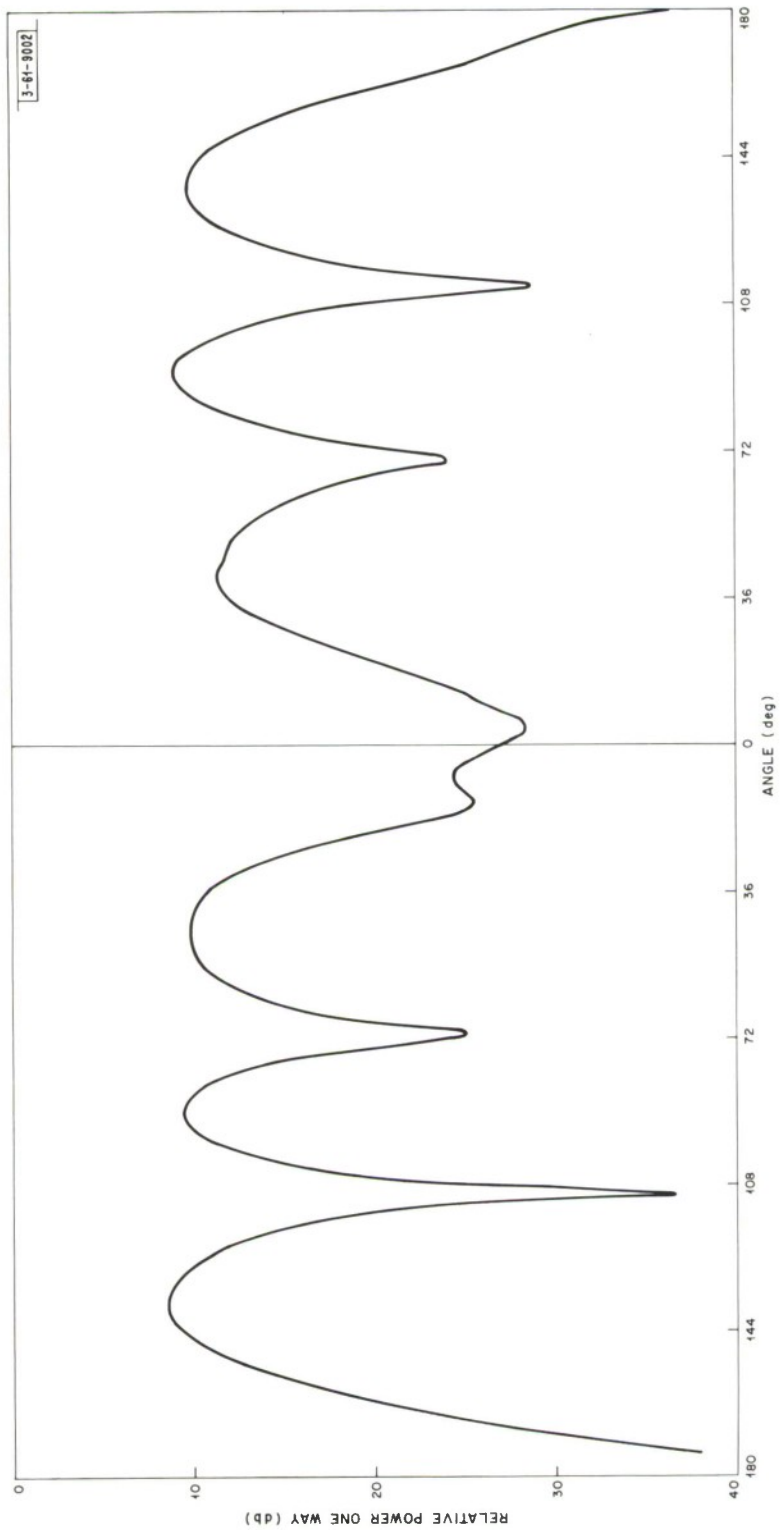

Fig. 18(c). Maximum RFI pattern.

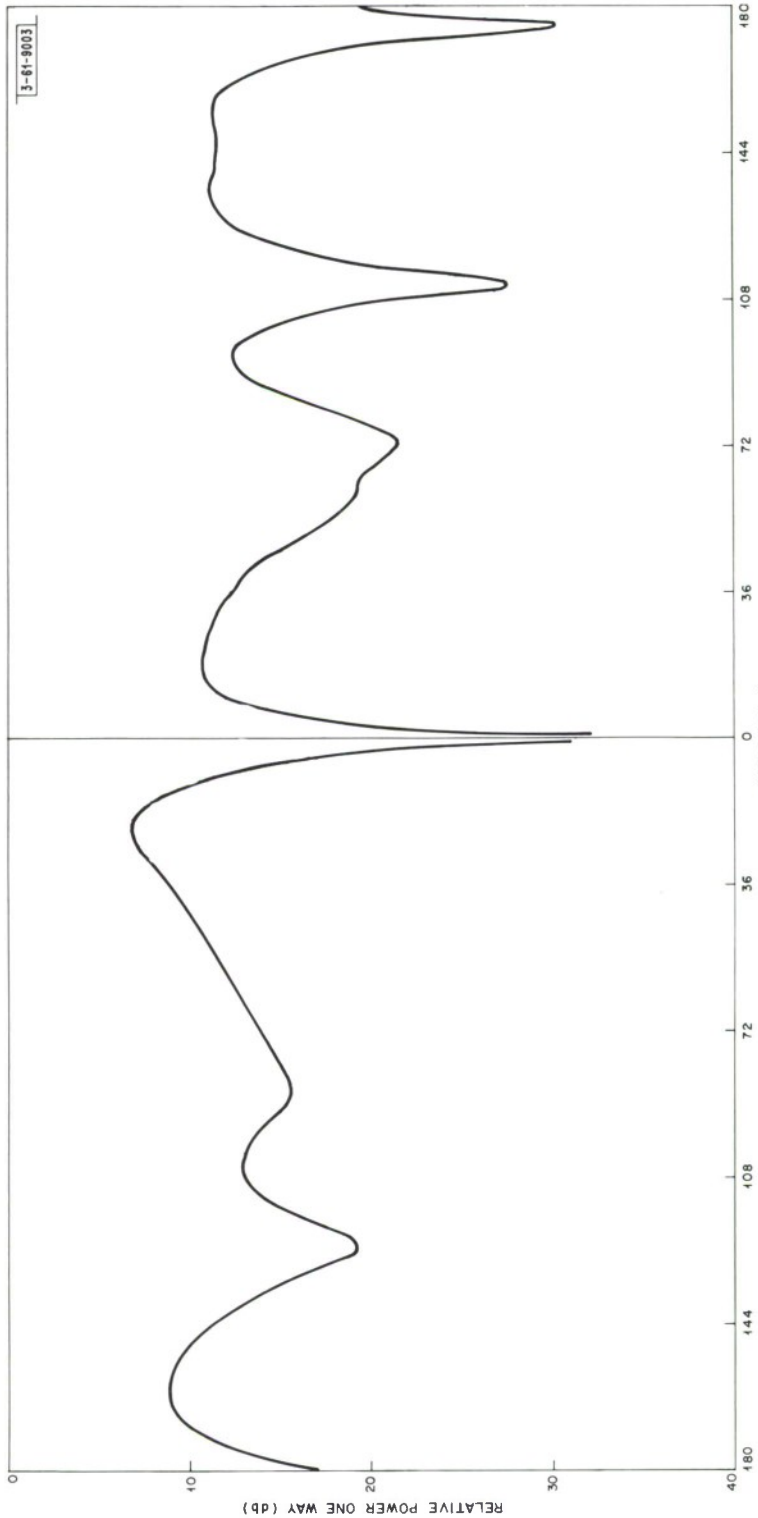

Fig. 19. Pattern of maximum RFI.

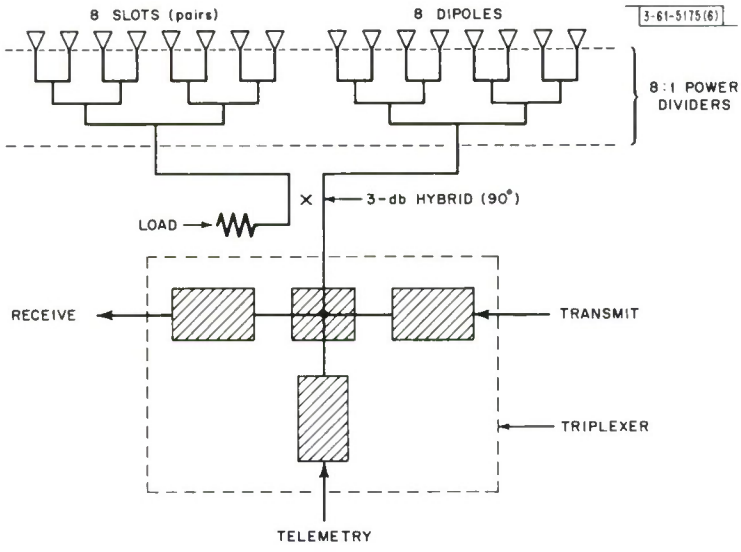

Fig. 20. Block diagram af LES-5 antenna feed netwark.

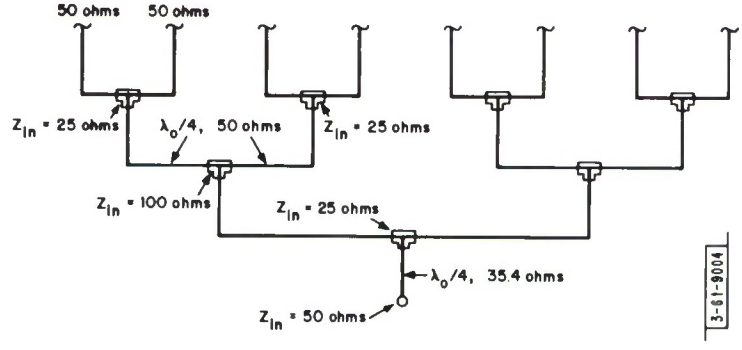

Fig. 21. Schematic diagram af power divider.

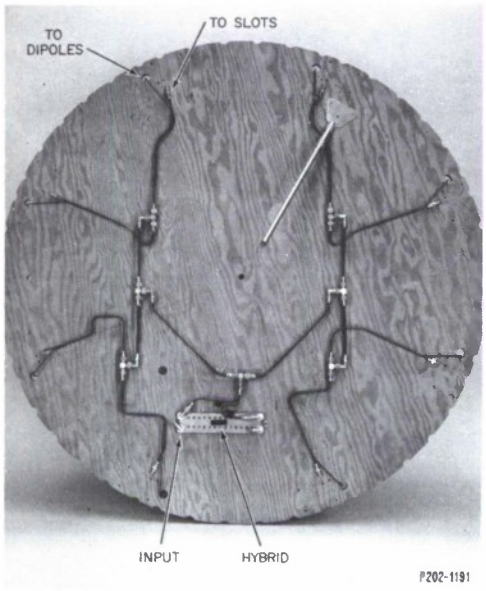

Fig. 22. Power dividers.

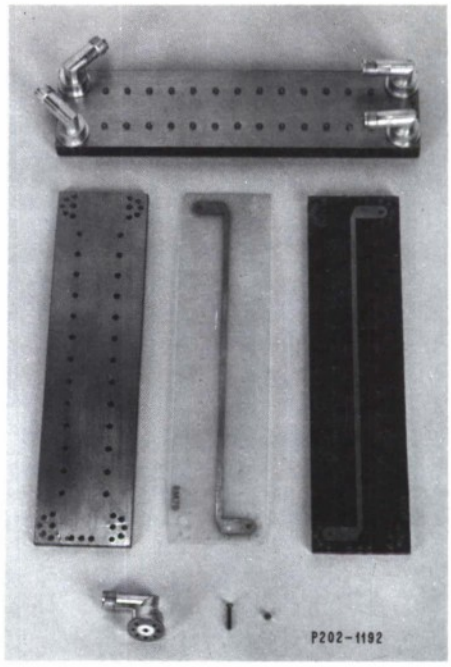

Fig. 23. 3-db hybrid (90°) junction.

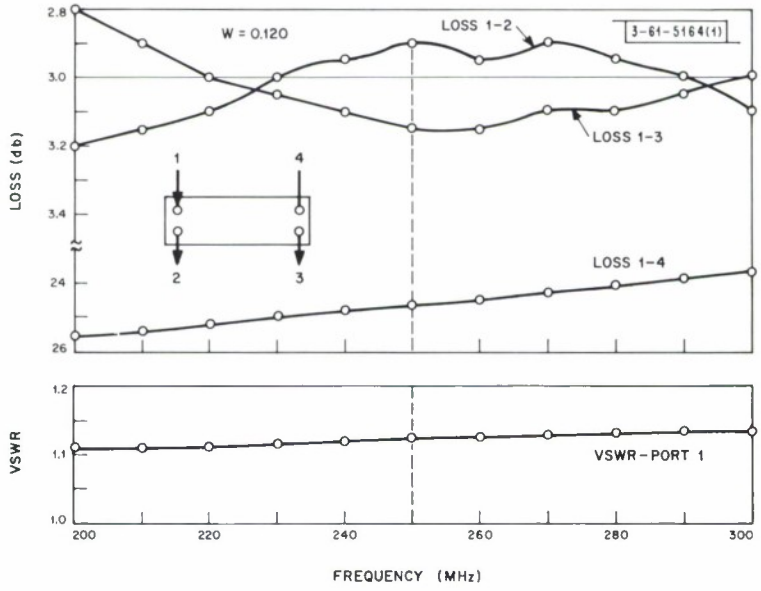

Fig. 24. 3-db power divider insertion loss and VSWR.

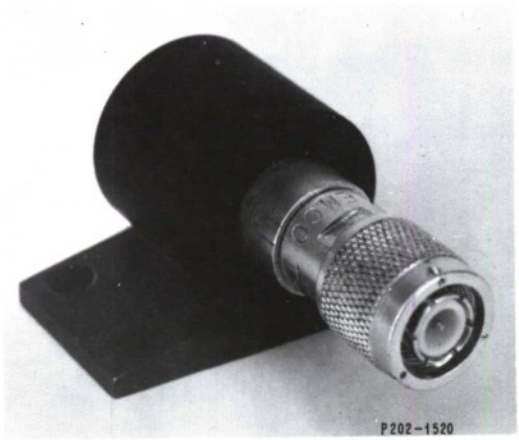

Fig. 25. Hybrid load.

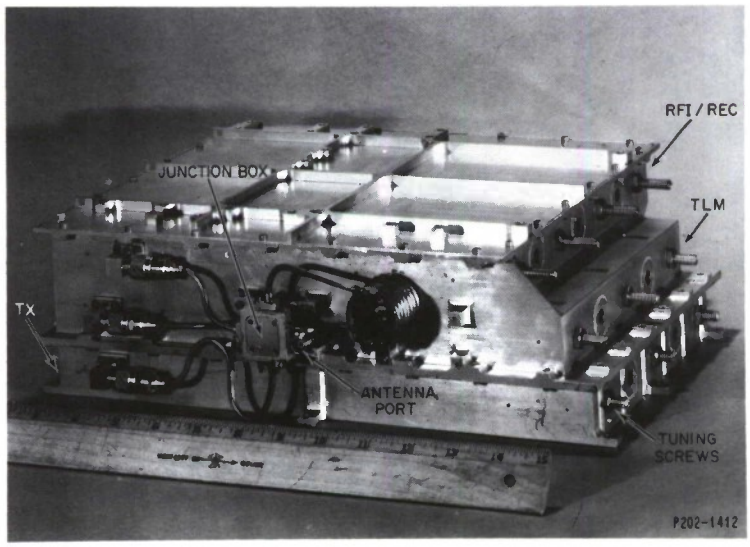

Fig. 26. LES-5 triplexer.

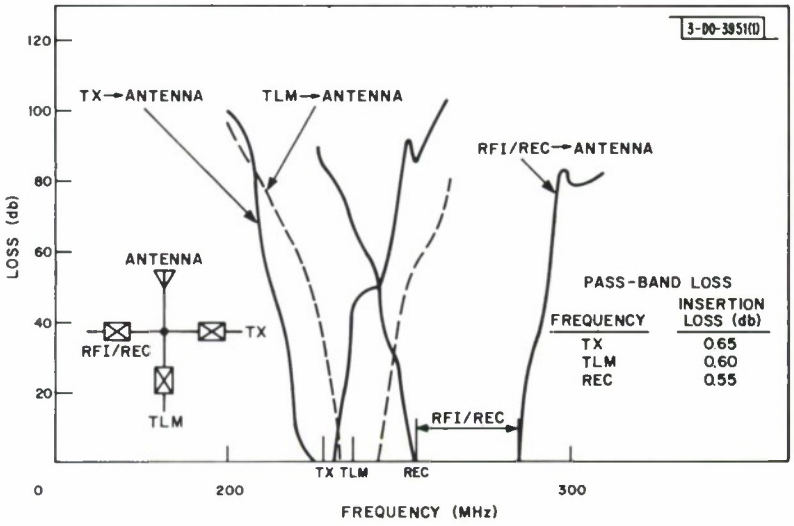

Fig. 27. Triplexer response curves.

Fig. 28. One-fifth scale model of LES-5.

Fig. 29. Satellite at Lincoln Laboratary's Antenna Test Range.

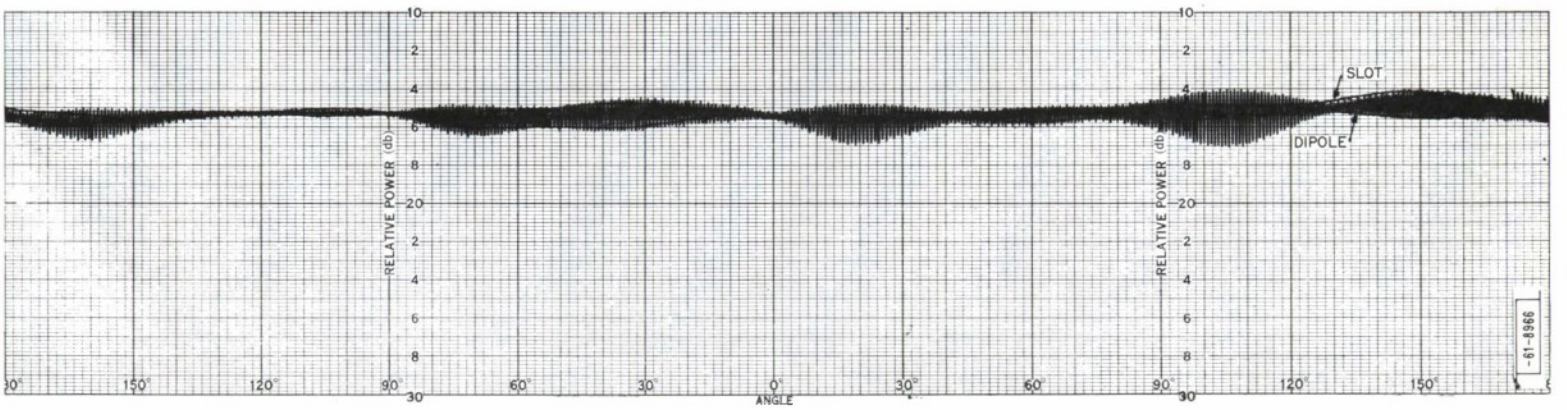

Fig. 30. Equatorial pattern, 13-foot range, $\theta = 90°$, TX.

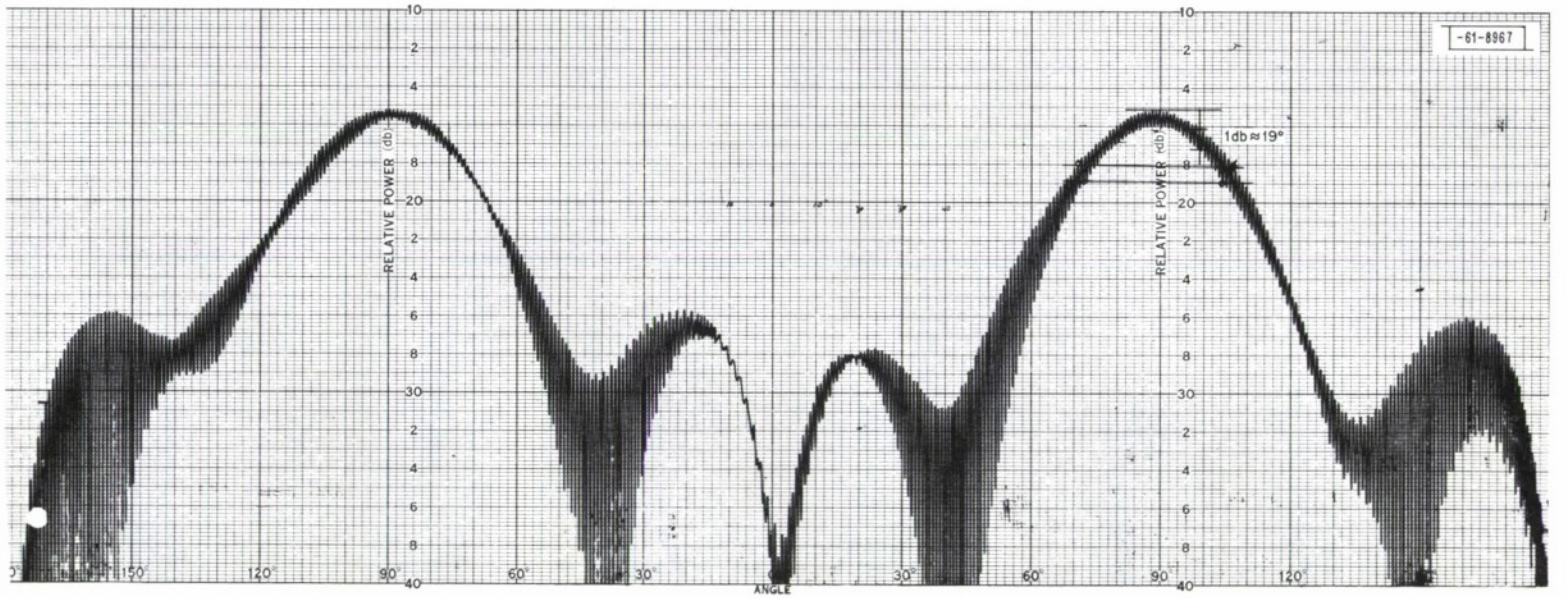

Fig. 31. Polar pattern, 13-foot range, TX.

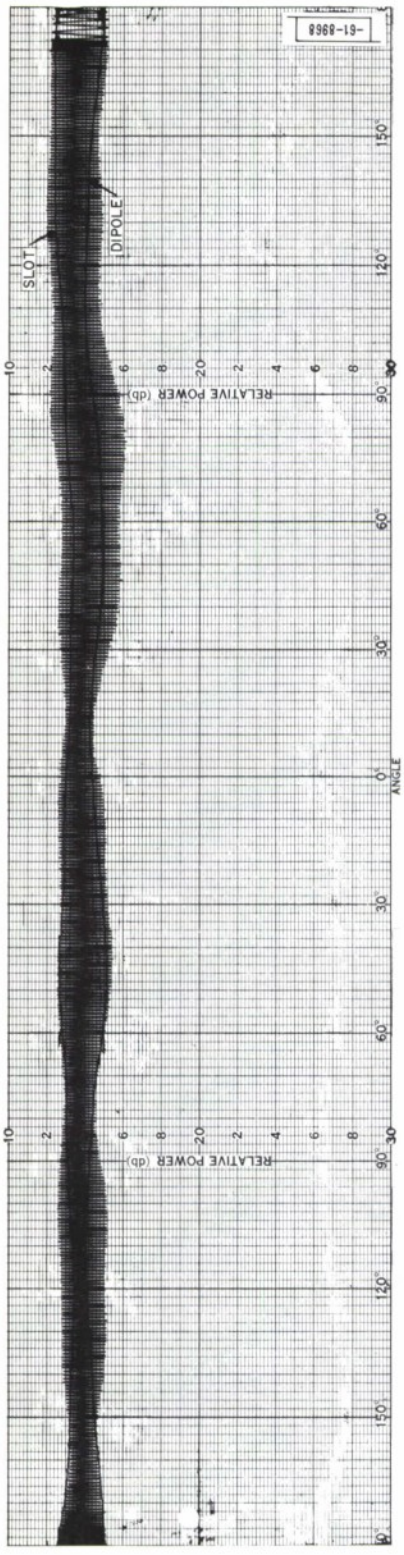

Fig. 32. Equatorial pattern, 14-foot range, θ = 90°, TX.

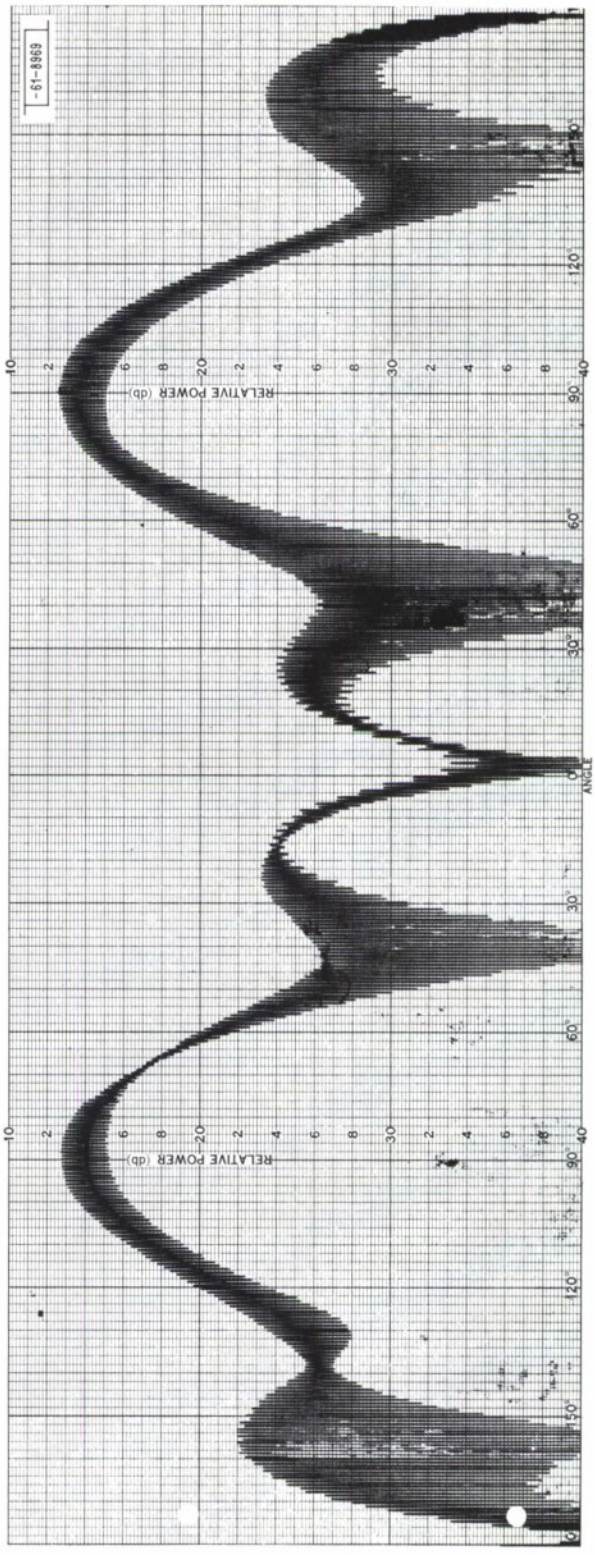

Fig. 33. Polar pattern, 14-foot range, TX.

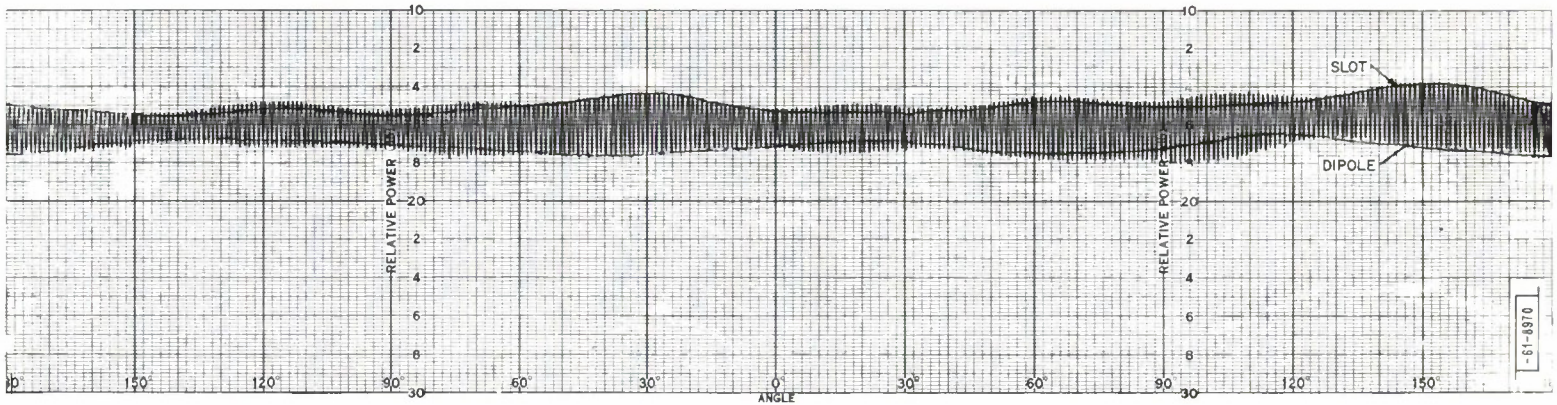

Fig. 34. Equatorial pattern, 15-foot range, θ = 90°, TX.

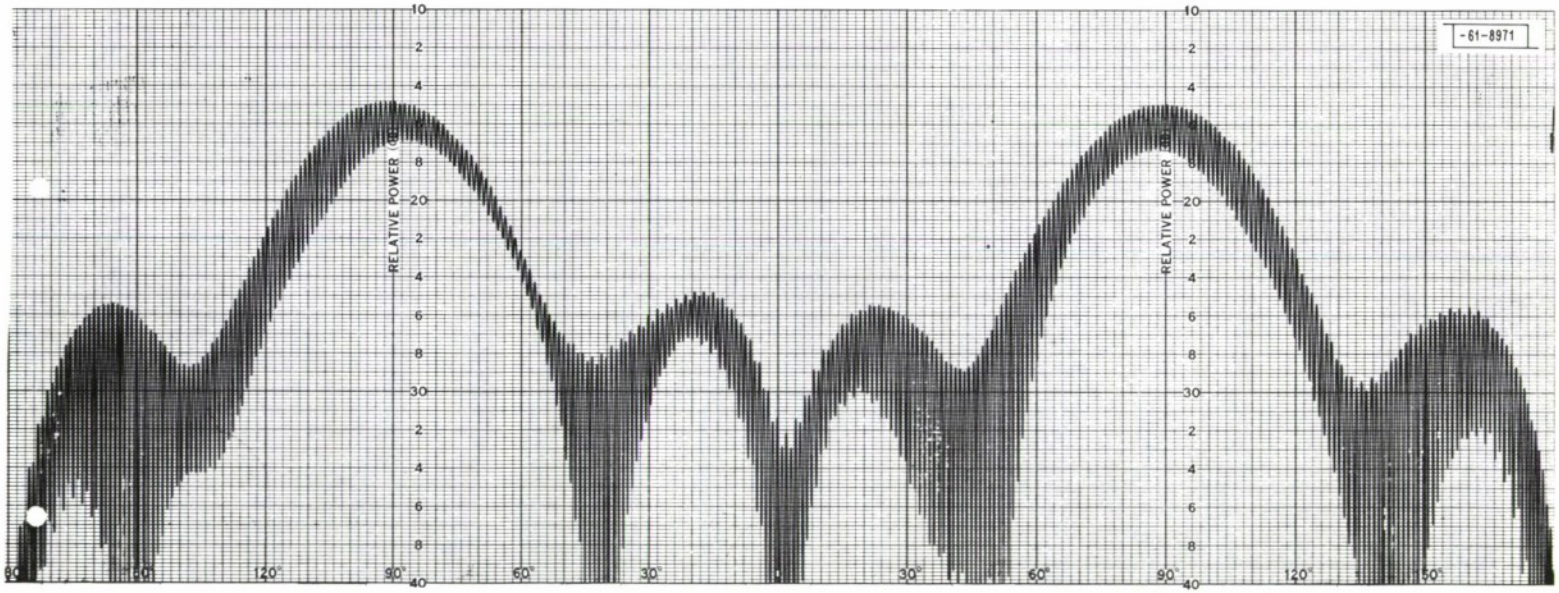

Fig. 35. Polar pattern, 15-foot range, TX.

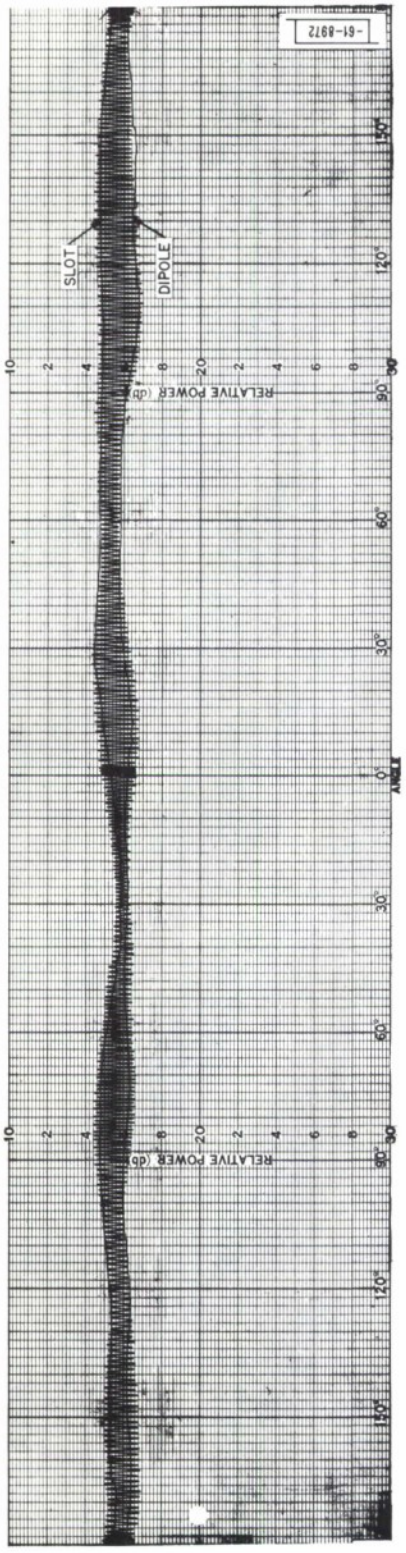

Fig. 36. Equatorial pattern, 13-foot range, θ = 90°, TLM.

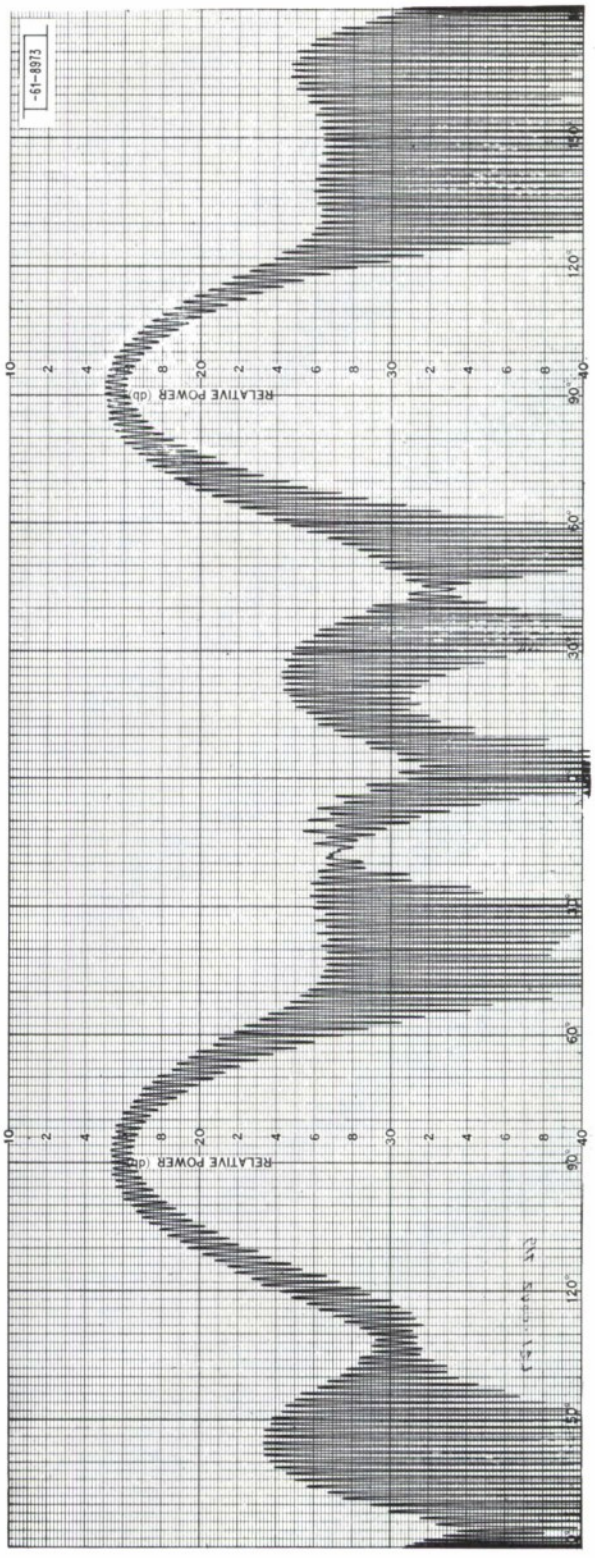

Fig. 37. Polar pattern, 13-foot range, TLM.

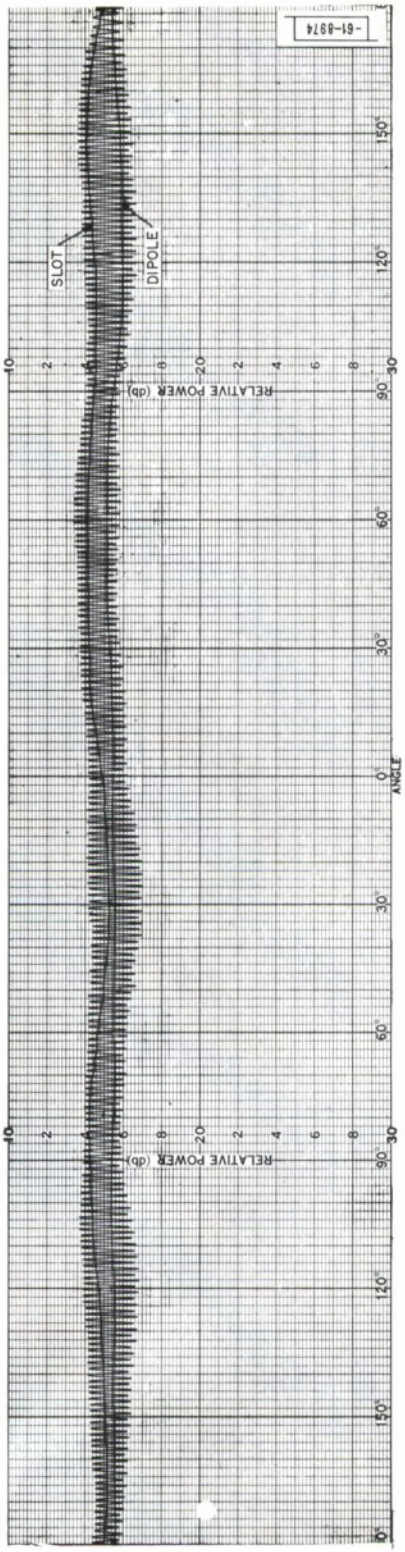

Fig. 38. Equatorial pattern, 14-foot range, $\theta = 90°$, TLM.

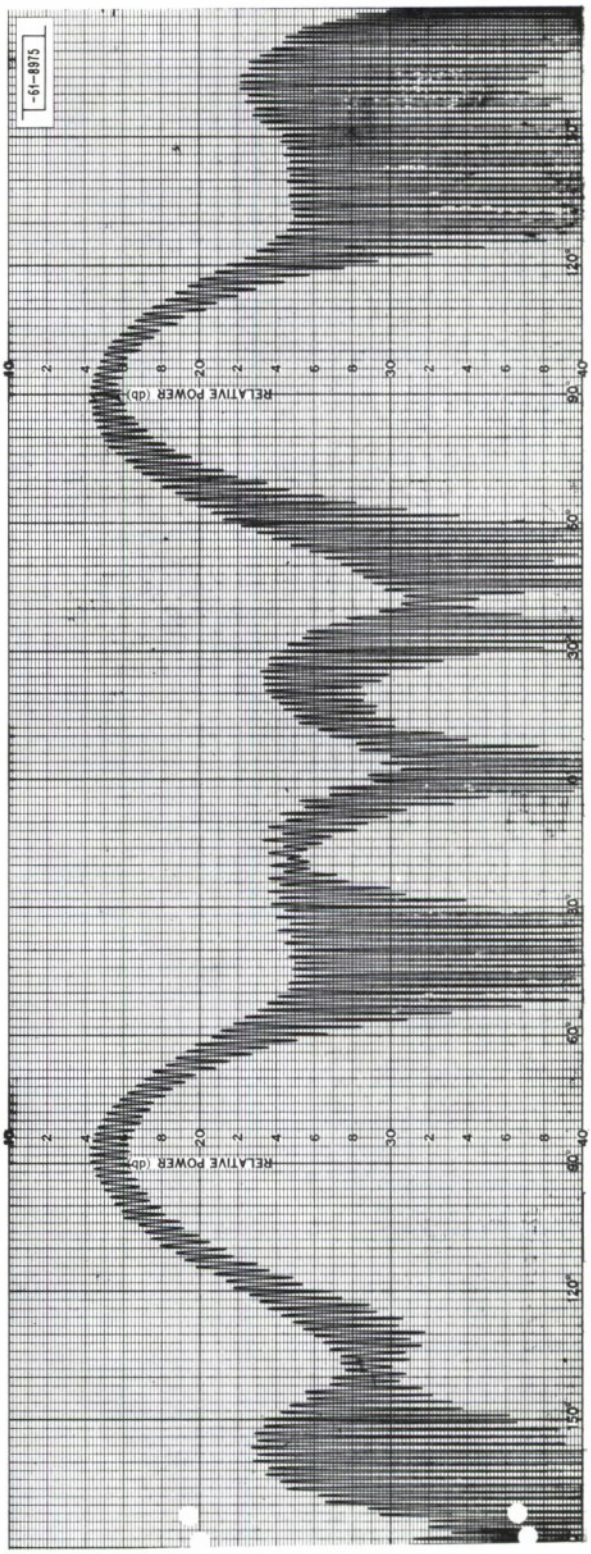

Fig. 39. Polar pattern, 14-foot range, TLM.

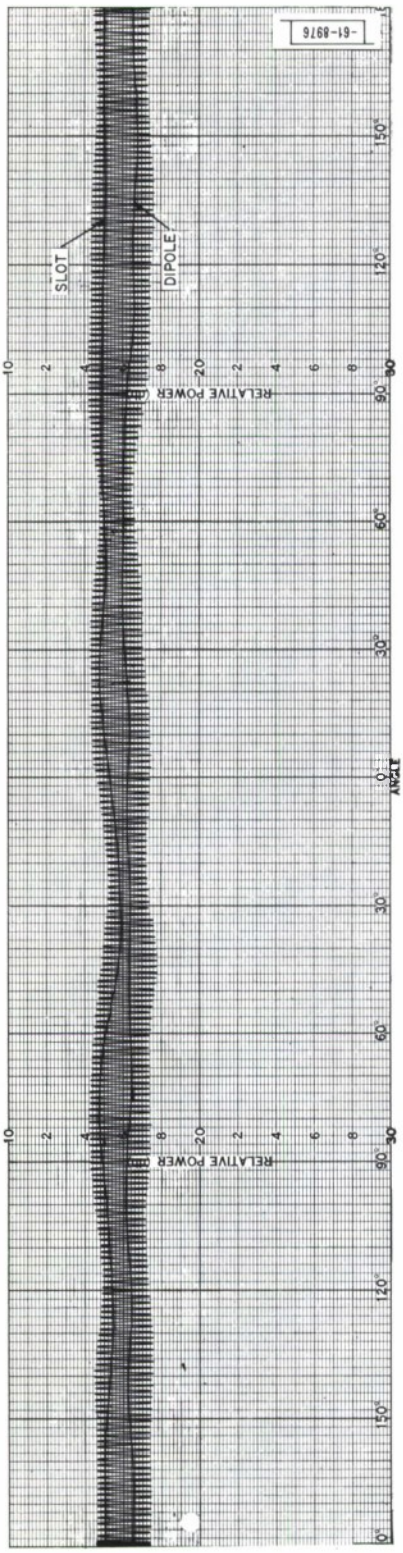

Fig. 40. Equatorial pattern, 15-foot range, θ = 90°, TLM.

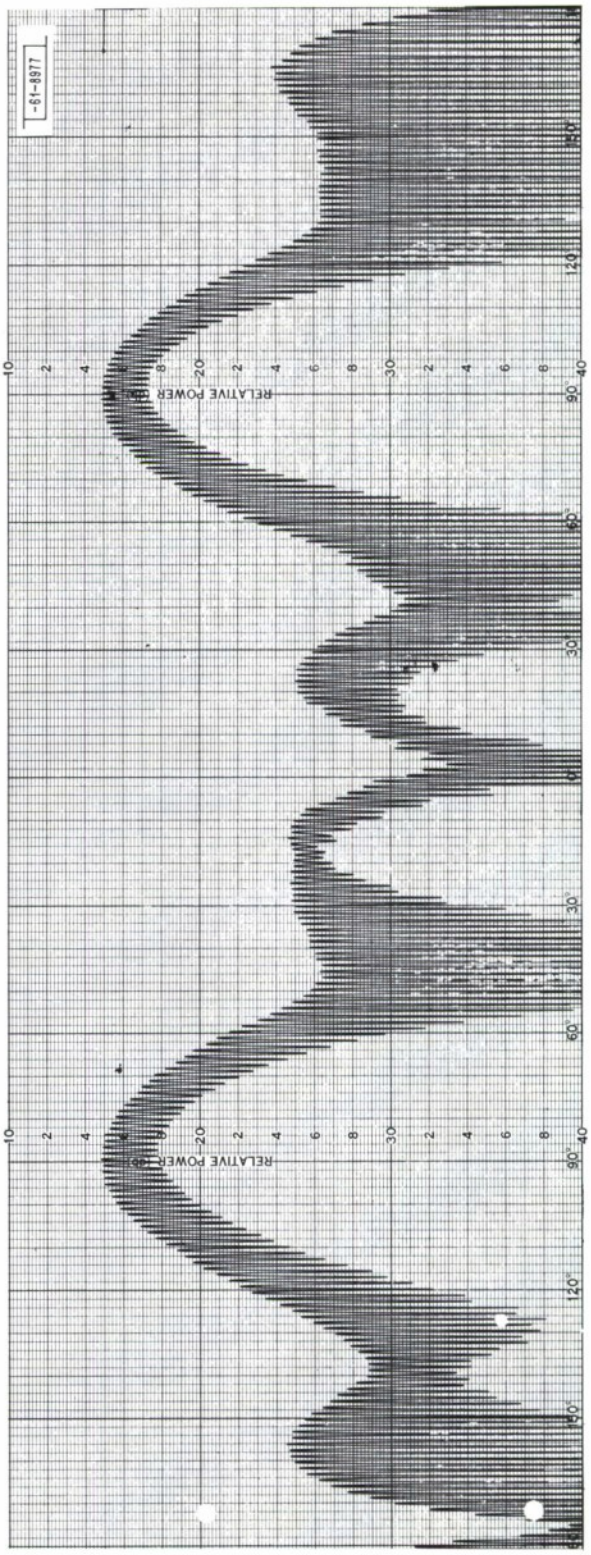

Fig. 41. Polar pattern, 15-foot range, TLM.

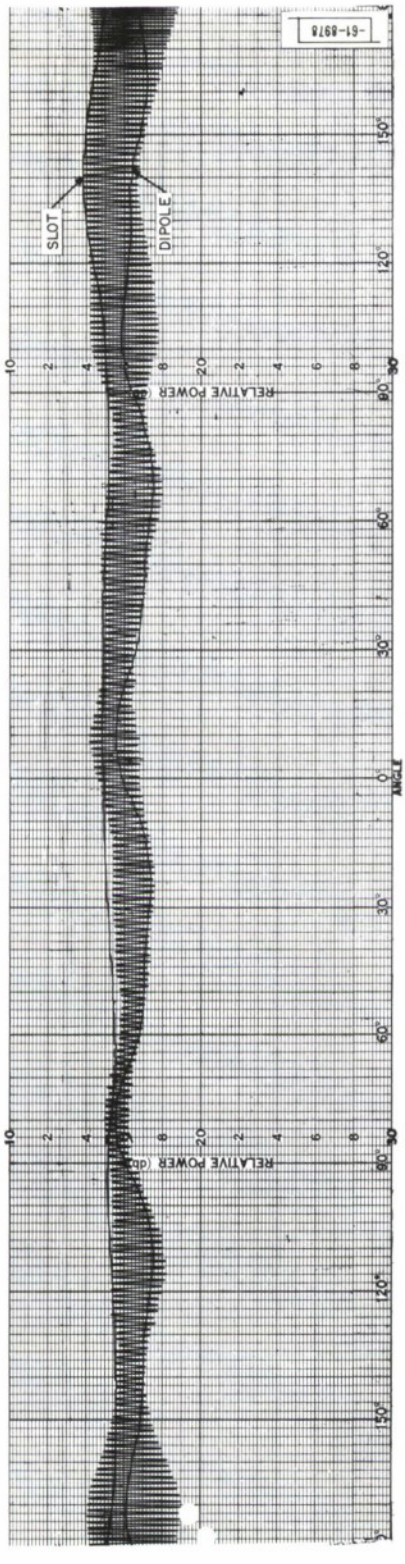

Fig. 42. Equatoriol pattern, 13-foot range, θ = 90°, REC.

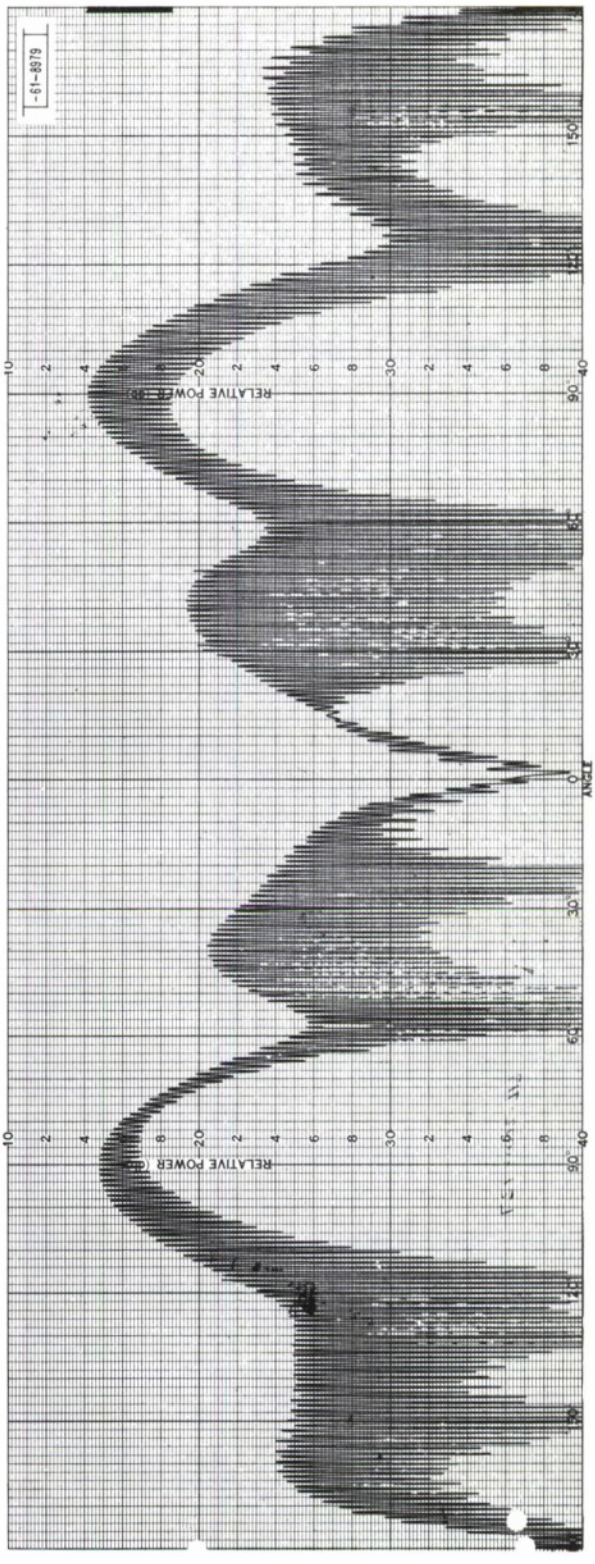

Fig. 43. Polor pattern, 13-foot ronge, REC.

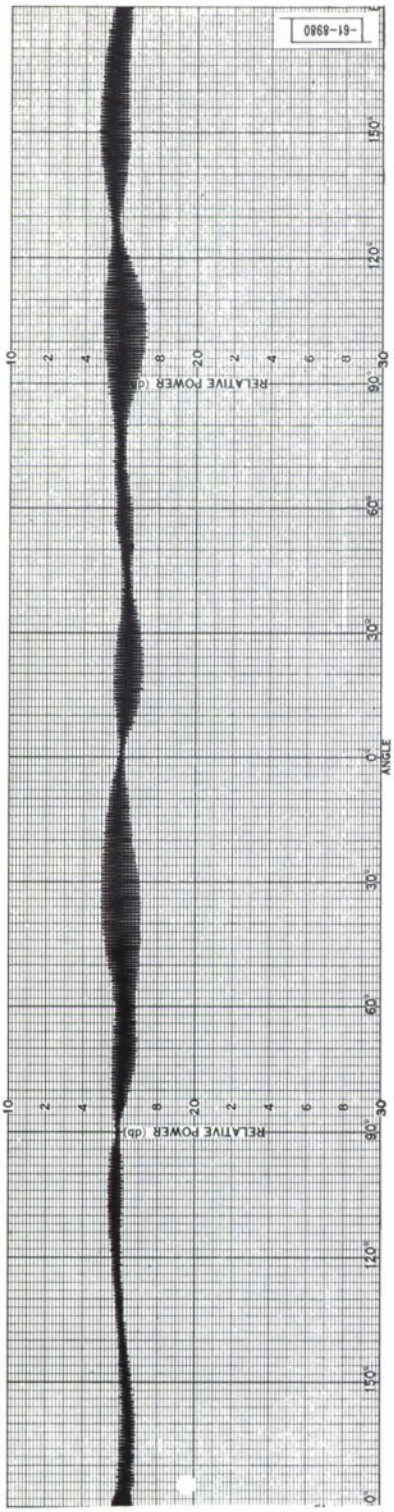

Fig. 44. Conical pattern, 13-foot range, θ = 83°, TX.

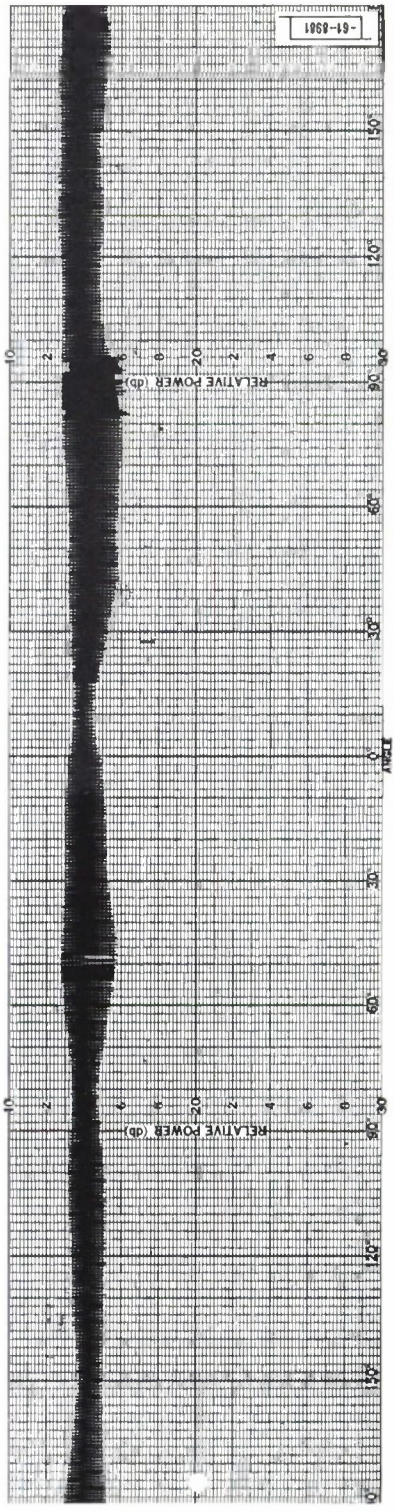

Fig. 45. Conical pattern, 14-foot range, θ = 83°, TX.

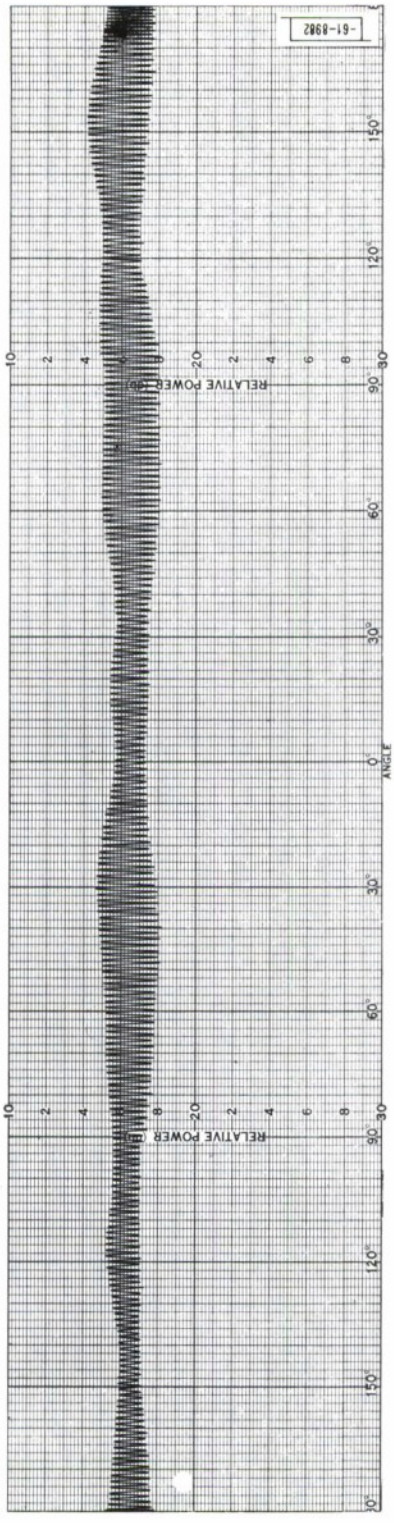

Fig. 46. Conical pattern, 15-foot range, θ = 83°, TX.

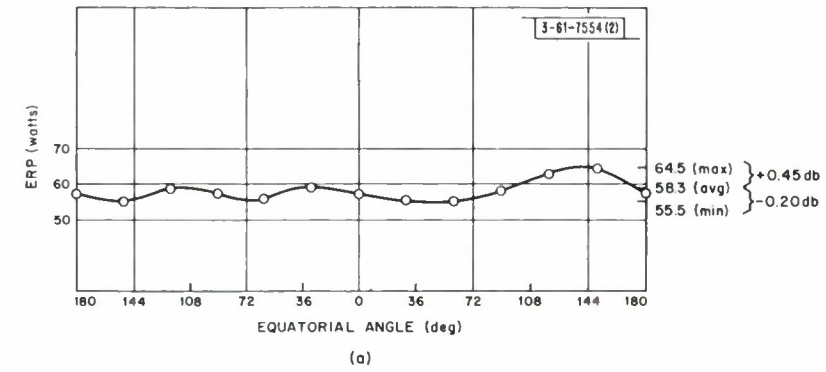

(a)

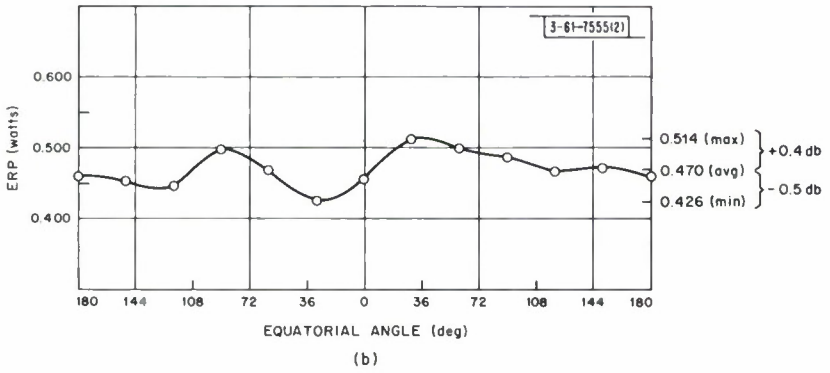

(b)

Fig. 47. Equatorial plane, circularly polarized ERP patterns (to matched polarization): (a) TX, and (b) TLM.

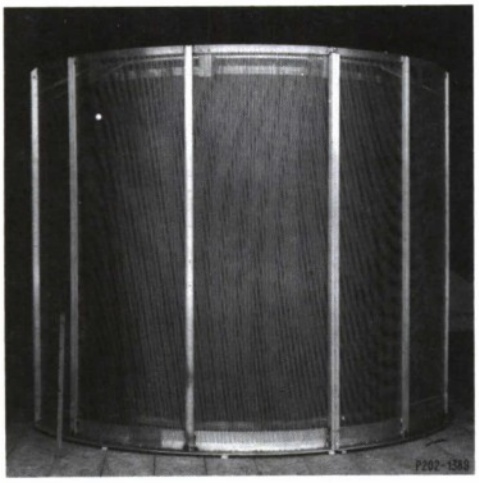

Fig. 48. Transportoble test chomber (TTC).

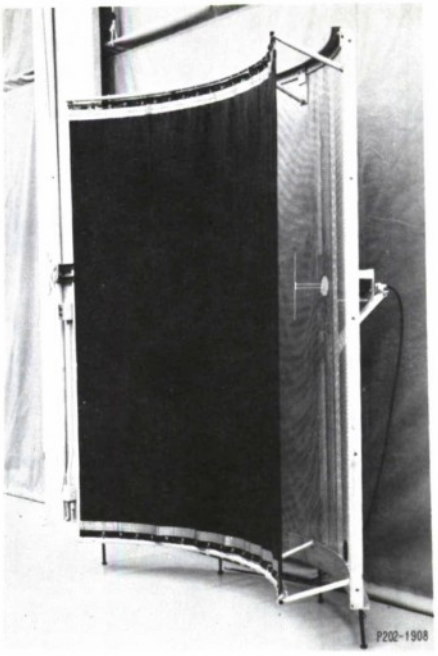

Fig. 49. Section of TTC.

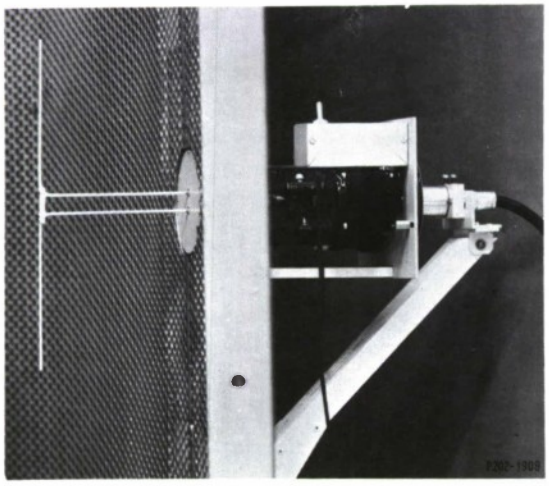

Fig. 50. Rototoble dipole probe in TTC.

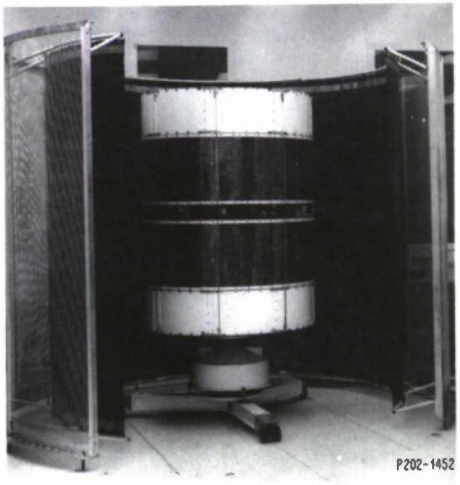

Fig. 51. LES-5 in TTC.

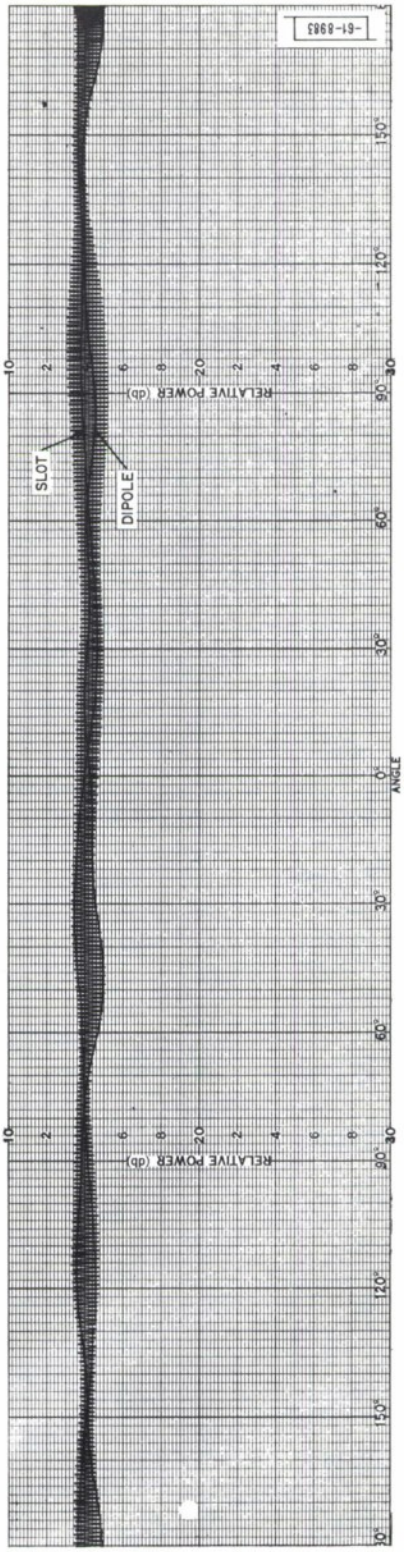

Fig. 52. Equatorial pattern at TX, LES-5 in TTC.

DOCUMENT CONTROL DATA – R&D

(Security classification of title, body of abstract and indexing annotation must be entered when the overall report is classified)

1. ORIGINATING ACTIVITY *(Corporate author)*
Lincoln Laboratory, M.I.T.

2a. REPORT SECURITY CLASSIFICATION
Unclassified

2b. GROUP
None

3. REPORT TITLE
Antenna System for LES-5

4. DESCRIPTIVE NOTES *(Type of report and inclusive dates)*
Technical Report

5. AUTHOR(S) *(Last name, first name, initial)*
Devane, Mark E.
Frediani, David J.
LaPage, Bernard F.
Rosenthal, Milton L.
Sotiropoulos, Arthur

6. REPORT DATE
18 July 1968

7a. TOTAL NO. OF PAGES
52

7b. NO. OF REFS
4

8a. CONTRACT OR GRANT NO.
AF 19(628)-5167

b. PROJECT NO.
649L

c.

d.

9a. ORIGINATOR'S REPORT NUMBER(S)
Technical Report 451

9b. OTHER REPORT NO(S) *(Any other numbers that may be assigned this report)*
ESD-TR-68-228

10. AVAILABILITY/LIMITATION NOTICES
This document has been approved for public release and sale; its distribution is unlimited.

11. SUPPLEMENTARY NOTES
None

12. SPONSORING MILITARY ACTIVITY
Air Force Systems Command, USAF

13. ABSTRACT

The antenna system for Lincoln Laboratory's fifth experimental satellite (LES-5) is described. This is the first circularly polarized VHF antenna to be tested on an orbiting satellite. Coverage is omnidirectional in the equatorial plane. Design considerations are discussed, development of the component dipole and slot array elements is explained, and performance data are given for the final flight configuration.

14. KEY WORDS

LES-5
VHF
dipole antennas
slot antennas
communications satellites
transponders
solid state
antenna radiation patterns
Salisbury Screen
circular polarization
Titan III-C